



# Vertical profiles of global tropospheric nitrogen dioxide (NO<sub>2</sub>) obtained by cloud-slicing TROPOMI

Rebekah P. Horner<sup>1</sup>, Eloise A. Marais<sup>1</sup>, Nana Wei<sup>1</sup>, Robert G. Ryan<sup>1,\*</sup>, Viral Shah<sup>2,3</sup>

5 <sup>1</sup>Department of Geography, University College London, London, UK

<sup>2</sup>Global Modeling and Assimilation Office (GMAO), NASA Goddard Space Flight Center, Greenbelt, MD 20770, USA

<sup>3</sup>Science Systems and Applications, Inc., Lanham, MD 20706, USA

\*Now at: School of Geography, Earth and Atmospheric Sciences, University of Melbourne, Melbourne, Australia

Correspondence to: Eloise A. Marais (e.marais@ucl.ac.uk); Rebekah P. Horner (rebekah.horner.20@ucl.ac.uk)

10 **Abstract.** Routine observations of the vertical distribution of tropospheric nitrogen oxides (NO<sub>x</sub> ≡ NO + NO<sub>2</sub>) are severely lacking, despite the large influence of NO<sub>x</sub> on climate, air quality, and atmospheric oxidants. Here we derive vertical profiles of global seasonal mean tropospheric NO<sub>2</sub> by applying the cloud-slicing method to TROPOMI columns of NO<sub>2</sub> retrieved above optically thick clouds. The resultant NO<sub>2</sub> are at a horizontal resolution of 1° × 1° for multiple years (June 2018 to May 2022) covering 5 layers in the upper (180-320 hPa and 320-450 hPa) and mid (450-15 600 hPa and 600-800 hPa) troposphere, and the marine boundary layer (800 hPa to the Earth's surface). Terrestrial boundary layer NO<sub>2</sub> are obtained as the difference between TROPOMI tropospheric columns and the integrated column of cloud-sliced NO<sub>2</sub> in all layers above the boundary layer. Cloud-slicing NO<sub>2</sub> is typically 20-60 pptv throughout the free troposphere and spatial coverage ranges from > 60% in the mid-troposphere to < 20% in the upper troposphere and boundary layer. Our product is similar (within 10-15 pptv) to NO<sub>2</sub> data from NASA DC-8 aircraft campaigns (INTEX-A, ARCTAS, SEAC<sup>4</sup>RS, ATom) 20 when both datasets are abundant and sampling coverage is commensurate, but such instances are rare. We use the cloud-sliced NO<sub>2</sub> to critique current knowledge of the vertical distribution of global NO<sub>2</sub>, as simulated with the GEOS-Chem chemical transport model updated to include peroxypropionyl nitrate (PPN) and aerosol nitrate photolysis that liberate NO<sub>2</sub> in the lower and mid-troposphere for aerosol nitrate photolysis and upper troposphere for PPN. Multiyear GEOS-Chem and cloud-sliced 25 means are compared to mitigate the influence of interannual variability. We find that for cloud-sliced NO<sub>2</sub> the interannual variability is ~10 pptv over remote areas and ~25 pptv over areas influenced by lightning and surface sources. The model consistently underestimates NO<sub>2</sub> across the remote marine troposphere by ~15 pptv. In the northern midlatitudes, GEOS-Chem overestimates mid-tropospheric NO<sub>2</sub> by 20-50 pptv, as NO<sub>x</sub> production per lightning flash is parameterised to be almost double the rest of the world. There is a critical need for in-situ NO<sub>2</sub> measurements in the tropical terrestrial troposphere to evaluate cloud-sliced NO<sub>2</sub> there. The model and cloud-sliced NO<sub>2</sub> discrepancies identified here need to be investigated further to ensure 30 confident use of models to understand and interpret factors affecting the global distribution of tropospheric NO<sub>x</sub>, ozone and other oxidants.



## 1 Introduction

In the troposphere, nitrogen oxides ( $\text{NO}_x \equiv \text{NO} + \text{NO}_2$ ) influence the formation of tropospheric ozone ( $\text{O}_3$ ), a greenhouse gas, and the hydroxyl radical (OH), the main atmospheric oxidant (Atkinson, 2000; Bloss et al., 2005). Due to its influence on OH,  $\text{NO}_x$  also indirectly affects the lifetime and abundance of the potent greenhouse gas methane (Wild et al., 2001) and non-methane volatile organic compounds that contribute to  $\text{O}_3$  and particulate matter pollution (Crutzen and Andreae, 1990; Karl et al., 2007; Marais et al., 2016).  $\text{NO}_x$  is directly emitted from high-temperature combustion of fossil fuels, from open and domestic burning of biomass, and from natural processes such as lightning and bacteria in soils (Dignon, 1992; Pickering et al., 1998; Jain et al., 2006; Vinken et al., 2014).  $\text{NO}_x$  also enters the upper layers of the troposphere via downwelling from the stratosphere (Poulida et al., 1996). The distribution of  $\text{NO}_x$  varies throughout the troposphere as a result of these sources and due to recycling of  $\text{NO}_x$  via oxidation, photolysis and thermal decomposition of gas- and aerosol-phase reservoirs of nitrogen (Chatfield, 1994; Moxim et al., 1996; Kotamarthi et al., 2001; Scharko et al., 2014). In the warm lower troposphere where anthropogenic sources dominate, the lifetime of  $\text{NO}_x$  is a few hours. This increases with altitude to several days in the cold, dry upper troposphere where  $\text{NO}_x$  is present mostly as NO (Travis et al., 2016), reservoir compounds dominate, and terminal loss of  $\text{NO}_x$  via wet deposition in the form of nitric acid ( $\text{HNO}_3$ ) is limited (Jaeglé et al., 1998).

Knowledge of the vertical distribution of tropospheric  $\text{NO}_x$  has been largely informed by in-situ instruments on research and commercial aircraft (Crawford et al., 1996; Brenninkmeijer et al., 1999; Bradshaw et al., 2000; Emmons et al., 2000; Petzold et al., 2015; Stratmann et al., 2016). These aircraft campaigns are few in time and space. The instruments used to measure  $\text{NO}_2$  are also susceptible to interference from decomposition of thermally unstable reservoir compounds of  $\text{NO}_x$  (Bradshaw et al., 2000; Browne et al., 2011; Reed et al., 2016). This interference is most severe in the upper troposphere and in remote marine regions where thermally labile  $\text{NO}_x$  reservoir compounds are abundant and decomposition of these compounds is promoted by the warm instrument inlet (Murphy et al., 2004; Nault et al., 2015; Shah et al., 2023). Studies now supplement these measurements with calculated daytime  $\text{NO}_2$  concentrations, as NO and  $\text{NO}_2$  can be assumed to be in photochemical steady state (PSS) (Davis et al., 1993; Crawford et al., 1996).

Networks of ground-based remote sensing instruments such as Multi Axis Differential Optical Absorption Spectroscopy (MAX-DOAS) and direct-sun Pandora instruments have expanded globally. Still, geographic coverage for both is mostly in the northern hemisphere (Verhoelst et al., 2021). For Pandora, only the total tropospheric column can be derived from total atmospheric column measurements (Pinaridi et al., 2020). MAX-DOAS, under ideal conditions, can retrieve up to four independent layers in the troposphere, though vertical extent at most sites excludes the upper troposphere (Tirpitz et al., 2021). Space-based remote sensing observations used to retrieve vertical column densities (VCDs) of tropospheric  $\text{NO}_2$  address limited spatial sampling of commercial and research aircraft and Pandora and MAX-DOAS networks by offering daily global coverage, but with only one piece of vertical information in the troposphere (Ryan et al., 2023). These satellite observations



65 are also impacted by biases in modelled vertical profiles of NO<sub>2</sub> required to retrieve VCDs (Verhoelst et al., 2021), in particular  
in the upper troposphere where satellite observations are most sensitive to tropospheric NO<sub>2</sub> (Boersma et al., 2004; Travis et  
al., 2016; Silvern et al., 2018; Shah et al., 2023).

Mixing ratios of NO<sub>2</sub> in distinct layers of the troposphere can be retrieved using so-called cloud-slicing. This technique targets  
70 partial columns (stratospheric + tropospheric) above clouds that are sufficiently optically thick that UV-visible instruments  
observe discrete layers in the troposphere. Cloud-slicing was first applied by Ziemke et al. (2001) to O<sub>3</sub> columns to derive  
seasonal multi-year mean upper tropospheric O<sub>3</sub> mixing ratios in the tropics. Cloud-slicing has since been used to retrieve  
seasonal mean concentrations of NO<sub>2</sub> from the Ozone Monitoring Instrument (OMI) in both the mid (900-650 hPa or 2-4 km)  
and upper (450-280 hPa or 6-11 km) troposphere at 5° latitude × 8° longitude (500 km × 800 km) as well as in six pressure  
75 levels (centred at 280, 380, 500, 620, 720 and 820 hPa) at 2° × 2° (Belmonte Rivas et al., 2015; Choi et al., 2014; Marais et  
al., 2018). The OMI cloud-sliced NO<sub>2</sub> data provide useful information at very coarse scales (20° × 32°, seasonal) (Marais et  
al., 2018) and are hindered by large data loss after 2007 when many satellite pixels became obscured by the row anomaly  
(Torres et al., 2018). More recently, the higher spatial resolution TROPospheric Monitoring Instrument (TROPOMI) has been  
used to derive NO<sub>2</sub> mixing ratios in the upper troposphere (450-180 hPa or 6-12 km) at finer scales than was possible with  
80 OMI of 1° × 1° (~100 km) (Marais et al., 2021). Cloud-sliced NO<sub>2</sub> from TROPOMI has so far only been derived for a single  
year, as at the time there were frequent updates to the retrieval that led to inconsistencies in the TROPOMI NO<sub>2</sub> VCDs used  
for cloud slicing. TROPOMI NO<sub>2</sub> data have since been reprocessed to obtain a consistent data record starting in May 2018.

Evaluation of cloud-sliced NO<sub>2</sub> data products is very limited, as coincidence of satellite observations and aircraft campaigns  
85 is rare. Choi et al. (2014) found that the NASA OMI mid tropospheric product is similar (<10% difference) to coincident  
research aircraft campaign observations, limited to Texas and the Pacific Ocean west of North America. Marais et al. (2021)  
intercompared seasonal mean cloud-sliced upper tropospheric NO<sub>2</sub> from TROPOMI and the NASA OMI product to identify  
that TROPOMI background values routinely exceed OMI by 12-26 pptv. Given these product disparities, independent  
evaluation of cloud-sliced NO<sub>2</sub> mixing ratios is crucial. Past (2006-2013) NASA DC-8 aircraft campaigns and the more recent  
90 (2016-2018) NASA DC-8 Atmospheric Tomography Mission (ATom) measurement campaign sampled the troposphere from  
close to the surface to the upper layers of the troposphere, offering the opportunity to evaluate cloud-sliced NO<sub>2</sub> mixing ratios  
over the remote Pacific and Atlantic Oceans (ATom) (Thompson et al., 2022), the Canadian Arctic during the Arctic Research  
of the Composition of the Troposphere from Aircraft and Satellites (ARCTAS) campaign (Jacob et al., 2010), and the eastern  
US during the Intercontinental Chemical Transport Experiment – North America Phase A (INTEX-A) (Singh et al., 2006) and  
95 the Studies of Emissions and Atmospheric Composition, Clouds and Climate Coupling by Regional Surveys (SEAC<sup>4</sup>RS) (Toon  
et al., 2016) campaigns.



100 Here we derive a global dataset of 4 years of seasonal multiyear mean concentrations of NO<sub>2</sub> in five discrete vertical layers in the troposphere from the planetary boundary layer to the upper troposphere. We evaluate our dataset against directly measured and calculated (PSS) NO<sub>2</sub> from multiple NASA DC-8 aircraft campaigns and go on to use the cloud-sliced data to assess current understanding of the global vertical distribution of tropospheric NO<sub>x</sub> as simulated by the GEOS-Chem chemical transport model.

## 2 Methods

### 2.1 Cloud-slicing TROPOMI NO<sub>2</sub> columns

105 TROPOMI was launched in October 2017 aboard the Sentinel-5P satellite. The initial TROPOMI nadir spatial resolution of 7.2 km × 3.5 km was enhanced to 5.6 km × 3.5 km in August 2019 (Liu et al., 2021). The swath width is 2600 km, resulting in daily global coverage at an equator crossing time of 13:30 local solar time (LST). To derive our cloud-sliced product, we use TROPOMI Level 2 swaths retrieved using a consistent algorithm (version 2.3.1). Data are available as the reprocessed (PAL) product from 1 June 2018 to 14 November 2021 (<https://data-portal.s5p-pal.com/>, last accessed 17<sup>th</sup> February 2022) and as the offline (OFFL) product from 14 November 2021 to 31 May 2022 (<https://s5phub.copernicus.eu/dhus/#/home>, last accessed 7 July 2022; now available at <https://dataspace.copernicus.eu/browser/>). The cloud-slicing approach was first applied to TROPOMI by Marais et al. (2021) to derive NO<sub>2</sub> mixing ratios in the upper troposphere over a broad pressure range from 450 to 180 hPa. We apply this cloud-slicing, with updates detailed below, to the whole troposphere to derive vertical profiles of seasonal mean NO<sub>2</sub> at the same 1° × 1° resolution as Marais et al. (2021) for multiple years (2018-2022) over five pressure ranges: one in the boundary layer below 800 hPa (<~2 km), two in the mid-troposphere at 800-600 hPa (~2-4 km) and 600-450 hPa (~4-6 km), and two in the upper troposphere at 450-320 hPa (~6-9 km) and 320-180 hPa (~9-12 km).

120 The first application of cloud-slicing to TROPOMI NO<sub>2</sub> is described in detail in Marais et al. (2021). We mostly follow the same approach. That is, pixels of individual swaths are filtered to isolate observations above optically thick clouds (cloud radiance fraction > 0.7). These are binned into cloud-top pressures within the 5 targeted pressure ranges on a fixed 1° × 1° grid. The stratospheric component of the total VCDs is corrected for a 13% underestimate in variance identified by Marais et al. (2021) from comparison to ground-based direct sun photometer Pandora measurements at the high-altitude (4.2 km) Mauna Loa site. The corrected stratospheric VCDs are multiplied by the reported stratospheric air mass factors (AMFs) to calculate stratospheric slant columns. The stratospheric slant columns are then subtracted from the total slant columns to estimate tropospheric slant columns that are converted to tropospheric VCDs using a geometric AMF. Only clusters of total above-cloud VCDs with a relatively uniform stratosphere are retained for cloud-slicing. These are identified as clusters of 1° × 1° pixels with a stratospheric column relative standard deviation < 0.02. A uniform stratosphere ensures that variability in partial NO<sub>2</sub> columns above optically thick clouds is dominated by variability in the troposphere. Cloud-slicing also requires that each



130 cluster include a representative range of cloud-top pressures (Choi et al., 2014). To ensure this is achieved, we remove clusters with cloud pressure ranges that are  $< 60\%$  of the pressure range of each layer (for example, 120 hPa threshold for the 800-600 hPa layer) and that have a large standard deviation ( $\geq 30$  hPa), informed by thresholds used by Choi et al. (2014) and Marais et al. (2018, 2021).

135 Next, we regress cloud-top pressures against above-cloud  $\text{NO}_2$  VCDs for clusters with at least 10 satellite pixels. We replace the reduced major axis (RMA) regression fit originally used by Marais et al. (2021) with Theil regression, as this reduces influence from outliers and is better suited to data that are not always normally distributed (Theil, 1950; Sen, 1968). The regression slope in molecules  $\text{cm}^{-2} \text{hPa}^{-1}$  is converted to  $\text{NO}_2$  volume mixing ratios in pptv as in Choi et al. (2014). The updated Theil regression fit addresses the 12-26 pptv overestimate in background values of cloud-sliced upper tropospheric  $\text{NO}_2$  identified by Marais et al. (2021) from comparison to the OMI upper tropospheric product. It also negates the need for the large TROPOMI free tropospheric column  $\text{NO}_2$  bias correction that Marais et al. (2021) used to resolve an apparent overestimate in TROPOMI compared to free tropospheric  $\text{NO}_2$  columns derived with measurements from Pandora and MAX-DOAS instruments at the high-altitude Izaña site. We also find that the outlier filter used by Marais et al. (2021) for cloud-sliced  $\text{NO}_2 > 200$  pptv is no longer needed, as it has negligible impact on seasonal mean cloud-sliced  $\text{NO}_2$  using our updated approach. As an initial assessment, we compare upper tropospheric cloud-sliced  $\text{NO}_2$  from our updated cloud-sliced approach to those from Marais et al. (2021). To ensure a consistent comparison, we recompute our updated cloud-sliced  $\text{NO}_2$  to cover the same pressure range (450-180 hPa) and time (June 2019 to May 2020) as Marais et al. (2021) and only compare  $1^\circ \times 1^\circ$  grids with 5 or more cloud-sliced data points in each data product.

150 The use of a geometric AMF to convert slant columns to vertical columns assumes  $\text{NO}_2$  mixing ratios within each layer are relatively well mixed. Belmonte Rivas et al. (2015) estimated that the difference between the geometric AMF and an AMF that accounts for surface reflectivity, the vertical  $\text{NO}_2$  profile and atmospheric scattering is  $< 10\%$  in all layers, except the lowest layer in that work of 770-870 hPa. In this lowest layer, equivalent to the top half of the boundary layer in our work, the difference in AMFs is up to  $\sim 30\%$ . The largest differences occur over land where  $\text{NO}_x$  emissions from sources such as urban traffic, industry, soils, and open burning of biomass cause an exponential increase in  $\text{NO}_2$  with pressure, unlike over the oceans where the  $\text{NO}_2$  profile is relatively uniform (Schreier et al., 2015; Wang et al., 2019; Kang et al., 2021; Shah et al., 2023). Given the steep vertical gradient in terrestrial boundary layer  $\text{NO}_2$ , we instead derive  $\text{NO}_2$  mixing ratios in the lowest layer over land as the difference between TROPOMI seasonal mean cloud-free  $\text{NO}_2$  tropospheric columns and free tropospheric columns obtained by integrating cloud-sliced  $\text{NO}_2$  over the four layers above the boundary layer (800-180 hPa).

160 Cloud fraction and cloud-top height data are from the improved Fast Retrieval Scheme for Clouds from the Oxygen A-band wide (FRESCO) algorithm called FRESCO-wide (Eskes and Eichmann, 2023). FRESCO-wide minimises the difference between measured and simulated spectra between 757-758, 760-761 and 765-770 nm and is so-called because the third spectral



165 window is wider than the 765-766 nm window used in the previous FRESCO-S algorithm (Wang et al., 2008; Van Geffen et al., 2022). The cloud-top pressure retrieved with FRESCO-wide corresponds to an altitude  $\sim 1$  km lower than the physical cloud-top height, as the cloud-top height retrieval assumes clouds are uniform reflective boundaries (Choi et al., 2014; Loyola et al., 2018). Marais et al. (2021) showed that cloud-sliced  $\text{NO}_2$  is relatively insensitive to the choice of TROPOMI cloud product. Their use of the TROPOMI Retrieval of Cloud Information using Neural Networks Cloud As Layers (ROCINN-CAL) product yielded upper tropospheric  $\text{NO}_2$  that was only 4-9 pptv more than that from the FRESCO-S product. The small difference results from an extratropical latitude-dependent divergence in cloud-top heights between the two products. The reprocessed TROPOMI  $\text{NO}_2$  product (v2.3.1) includes data from two cloud retrieval algorithms, FRESCO-wide and  $\text{O}_2\text{-O}_2$  cloud (O22CLD). FRESCO-wide is used here, as we find that it yields greater data density than the O22CLD product and differences in  $\text{NO}_2$  between the two products for coincident grids are small ( $< 10\%$ ). As of August 2023, ROCINN-CAL had not been reprocessed to obtain a consistent record, so is not used.

## 2.2 NASA DC-8 aircraft observations used to evaluate cloud-sliced $\text{NO}_2$

175 We evaluate our cloud-sliced  $\text{NO}_2$  against NASA DC-8 campaign data. To mitigate interference from decomposition of  $\text{NO}_x$  reservoir compounds on measured  $\text{NO}_2$  over remote regions, we calculate PSS  $\text{NO}_2$  for ATom measurements over remote oceans and for all measurements made in the upper troposphere. The PSS  $\text{NO}_2$  calculation assumes a dynamic daytime equilibrium between  $\text{NO}$  and  $\text{NO}_2$  resulting from the balance between photolysis of  $\text{NO}_2$  yielding  $\text{NO}$  and reaction of  $\text{NO}$  with oxidants regenerating  $\text{NO}_2$ . Silvern et al. (2018) estimated with GEOS-Chem that oxidation of  $\text{NO}$  in the southeast US upper troposphere was mostly (75%) by  $\text{O}_3$  followed by the hydroperoxy radical ( $\text{HO}_2$ ) (15%). The remaining 10% is due to oxidation by the methyl peroxy radical ( $\text{CH}_3\text{O}_2$ ) and halogen monoxides. Given dominance of  $\text{O}_3$  and  $\text{HO}_2$  and availability of measurements of these for almost all campaigns used, we calculate PSS  $\text{NO}_2$  as follows:

$$\text{NO}_2 = \text{NO} \times \left( \frac{k_1[\text{O}_3] + k_2[\text{HO}_2]}{j_{\text{NO}_2}} \right) \quad (1)$$

185

where  $j_{\text{NO}_2}$  is the  $\text{NO}_2$  photolysis frequency (in  $\text{s}^{-1}$ ) and  $k$  is the rate constant for oxidation of  $\text{NO}$  by  $\text{O}_3$  ( $k_1$ ) and by  $\text{HO}_2$  ( $k_2$ ) (in  $\text{cm}^3 \text{ molecule}^{-1} \text{ s}^{-1}$ ). The square brackets denote concentrations of  $\text{O}_3$  and  $\text{HO}_2$  in molecules  $\text{cm}^{-3}$ .  $\text{NO}$  and  $\text{NO}_2$  are in pptv. Values of  $j_{\text{NO}_2}$ ,  $\text{NO}$ ,  $[\text{O}_3]$ , and  $[\text{HO}_2]$  are from direct measurements and  $k_1$  and  $k_2$  are calculated using the temperature-dependent Arrhenius equations documented in the Jet Propulsion Laboratory (JPL) Chemical Kinetics and Photochemical Data publication number 19 (Burkholder et al., 2020). These for cold upper tropospheric temperatures ( $\sim 220$  K) are  $k_1 = 1.2 \times 10^{14} \text{ cm}^3 \text{ molecule}^{-1} \text{ s}^{-1}$  and  $k_2 = 1.1 \times 10^{13} \text{ cm}^3 \text{ molecule}^{-1} \text{ s}^{-1}$ . Only aircraft data obtained between 12:00 and 15:00 LST, 1.5 hours around the TROPOMI overpass time of 13:30 LST, are used, to ensure consistent sampling of the midday atmosphere and that the PSS assumption is valid. We remove aircraft data influenced by stratospheric air, identified as  $\text{O}_3/\text{CO} > 1.25 \text{ mol}$





mol<sup>-1</sup>. We also only use aircraft NO data to calculate PSS NO<sub>2</sub> if the NO measured is double the NO instrument detection limit  
195 of 6 pptv. This ensures measurements used are distinct from background noise in our PSS calculation (Ryerson et al., 2000;  
Yang et al., 2023).

NASA DC-8 aircraft campaigns with direct observations of NO<sub>2</sub> and observations needed to calculate PSS NO<sub>2</sub> include  
INTEX-A in summer 2004 over the United States (Singh et al., 2006), ARCTAS in spring and summer 2008 over the Canadian  
200 Arctic (ARCTAS Science Team, 2011), SEAC<sup>4</sup>RS in summer and autumn 2013 over the southeast US (SEAC<sup>4</sup>RS Science  
Team, 2014), and ATom once in all seasons from 2016 to 2018 following the same pole-to-pole flight path over the Atlantic  
and Pacific Oceans (ATom Science Team, 2021). Direct NO<sub>2</sub> measurements are from thermal-dissociation laser induced  
fluorescence (TD-LIF) (Di Carlo et al., 2013) for INTEX-A and from chemiluminescence (Ryerson et al., 2000) for all other  
campaigns. There are other DC-8 aircraft campaigns, such as the Subsonic Assessment Ozone and NO<sub>x</sub> Experiment (SONEX)  
205 over the North Atlantic and the Deep Convective Cloud and Chemistry (DC-3) over the eastern US. These are not included in  
our comparison, because SONEX has routine influence of stratospheric air (Fuelberg et al., 2000) and because DC-3 targeted  
thunderstorms with large concentrations of NO<sub>x</sub> from lightning, so is not representative of a standard atmosphere (Singh et al.,  
1999; Barth et al., 2015; Nault et al., 2016). Measurements of HO<sub>2</sub> are not available for SEAC<sup>4</sup>RS, so the PSS NO<sub>2</sub> calculation  
for this campaign uses average upper tropospheric [HO<sub>2</sub>] from the other three campaigns. We find that INTEX-A  
210 measurements of NO yield median PSS NO<sub>2</sub> values at 450-180 hPa that are anomalously large (150-450 pptv) in comparison  
to PSS NO<sub>2</sub> from SEAC<sup>4</sup>RS (30-130 pptv), so no upper tropospheric INTEX-A values are used.

### 2.3 The GEOS-Chem chemical transport model

We use GEOS-Chem to evaluate contemporary knowledge of tropospheric NO<sub>x</sub> by comparison to our cloud-sliced NO<sub>2</sub> vertical  
profiles. For this, we use GEOS-Chem version 13.3.4 (<https://doi.org/10.5281/zenodo.5764874>; accessed 11 May 2022) to  
215 calculate 4-year seasonal mean NO<sub>2</sub> covering the same vertical ranges as cloud-sliced NO<sub>2</sub>. Model years sampled (1 December  
2015 to 30 November 2019) are different to those for TROPOMI, due to a lag in availability of emission inventory data. The  
model is driven with NASA Modern Era Retrospective analysis for Research and Applications, version 2 (MERRA-2)  
reanalysis meteorology at a horizontal resolution of 2° × 2.5° over 47 vertical layers (30-35 in the troposphere) extending to  
0.01 hPa.

220

Global emissions of all anthropogenic sources except aircraft are from the Community Emissions Data System (CEDS) version  
2 for 2015 to 2019 (McDuffie et al., 2020). Aircraft emissions of NO<sub>x</sub> are from the Aviation Emissions Inventory Code (AEIC)  
for 2005 (Stettler et al., 2011). We use offline grid-independent soil NO<sub>x</sub> emissions from Weng et al. (2020), the online Global  
Fire Emissions Database version 4 with small fires (GFED4s) (van der Werf et al., 2017) inventory for open burning of  
225 biomass, and offline grid-independent lightning NO<sub>x</sub> emissions prepared by Meng et al. (2021) using the parameterisation  
detailed in Murray et al. (2012).



GEOS-Chem exhibits a known underestimate in tropospheric NO<sub>2</sub> over global oceans, as evidenced by past studies (Guo et al., 2023; Travis et al., 2020; Shah et al., 2023). We address this by updating the GEOS-Chem chemical mechanism to include  
230 photolysis of particle-phase nitrates (pNO<sub>3</sub>) liberating NO<sub>x</sub> as NO<sub>2</sub> and as the reservoir compound nitrous acid (HONO) followed by its prompt photolysis to form NO (Andersen et al., 2023; Kasibhatla et al., 2018; Romer et al., 2018; Ye et al., 2017). Photolysis of pNO<sub>3</sub> is implemented in GEOS-Chem by scaling the photolysis of nitric acid (HNO<sub>3</sub>) by an enhancement factor (EF). The EF is 100 for coarse-mode pNO<sub>3</sub> and is scaled down using the relative molar concentrations of pNO<sub>3</sub> and sea salt aerosol as in Shah et al. (2023) for fine-mode pNO<sub>3</sub>. This increases lower tropospheric (< 6 km) NO<sub>2</sub> over the remote  
235 ocean by up to 15 pptv, but has a smaller effect (< 10 pptv increase) above 6 km where pNO<sub>3</sub> is much less abundant (Shah et al., 2023). Photolysis of the NO<sub>x</sub> reservoir compound peroxypropionyl nitrate (PPN, C<sub>2</sub>H<sub>5</sub>C(O)OONO<sub>2</sub>) leading to formation of NO<sub>2</sub> occurs in the atmosphere, but is absent in GEOS-Chem. There are no reported laboratory measurements of NO<sub>2</sub> quantum yields from PPN. According to the Harwood et al. (2003) laboratory study, PPN absorption cross sections and quantum yields of the nitrate radical (NO<sub>3</sub>) are within 10% of peroxyacetyl nitrate (PAN, CH<sub>3</sub>C(O)OONO<sub>2</sub>), so we use PAN  
240 quantum yields and cross sections from Burkholder et al. (2020) to represent PPN photolysis in GEOS-Chem.

For consistent comparison of the model to cloud-sliced NO<sub>2</sub>, GEOS-Chem is sampled around the TROPOMI overpass (12:00-15:00 LST) following a 3-month spin-up from 1 September to 30 November 2015 for chemical initialisation of the 4-year simulation. Tropospheric NO<sub>2</sub> in GEOS-Chem is identified using MERRA-2 tropopause heights and additional filtering is  
245 applied to remove stratospheric intrusions (O<sub>3</sub>/CO > 1.25 mol mol<sup>-1</sup>). All-sky model scenes are sampled. Marais et al. (2021) determined by applying cloud-slicing to synthetic columns of NO<sub>2</sub> simulated with GEOS-Chem that the difference between NO<sub>2</sub> under very cloudy and all-sky conditions is small (< 17%). The TROPOMI cloud-sliced data are gridded to the GEOS-Chem grid for the comparison and only grid cells with at least 10 cloud-sliced data points are compared.

### 3 Results and Discussion

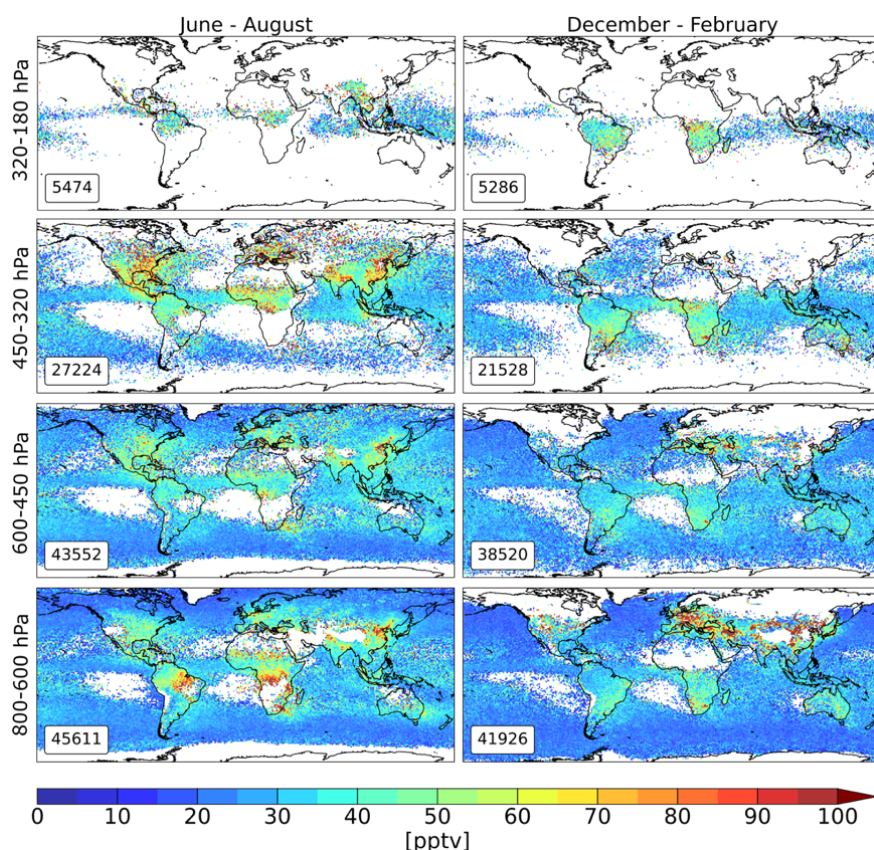
#### 250 3.1 Vertical distribution of tropospheric NO<sub>2</sub> from cloud-slicing TROPOMI

Fig. 1 shows the spatial distribution of cloud-sliced NO<sub>2</sub> in the free troposphere in June-August (JJA) 2018-2021 and December-February (DJF) 2018-2022 and Fig. 2 shows boundary-layer NO<sub>2</sub> (below 800 hPa) for the same seasons and years obtained with cloud-slicing over the ocean and differencing over land (Sect. 2.1). The percent filled global 1° × 1° grids is similar in both seasons, though with expected seasonal shifts in regions covered, due to seasonality in the location of clouds  
255 associated with convective features such as the Intertropical Convergence Zone (ITCZ) and absence of clouds over regions of persistent subsidence west of southern Africa and South America. Coverage is greatest in the mid-troposphere and least at 320-180 hPa. Percent coverage averaged over JJA and DJF is 63% of grid cells for 600-450 hPa and 68% for 800-600 hPa covering most of the tropics, subtropics, and midlatitudes. Slightly fewer (38%) result at 450-320 hPa, decreasing to 8% at





320-180 hPa. The few grid squares that are filled at this height mostly occur in the tropics, due to the higher tropopause and  
 260 greater abundance of optically thick clouds (Wang et al., 1996). In the boundary layer (Fig. 2), a total of ~14% of the grids are  
 filled, ~11% for direct cloud-slicing and ~3% for differencing. The latter is limited to locations over land with cloud-sliced  
 NO<sub>2</sub> in the top upper troposphere layer. Per-layer percent grids filled is similar for March-May and September-November.



265 **Figure 1:** Seasonal mean NO<sub>2</sub> in the free troposphere obtained by cloud-slicing TROPOMI. Columns are June-August (JJA; left)  
 and December-February (DJF; right) multiyear (2018-2021 for JJA, 2018-2022 for DJF) means at 1° × 1°. Rows from top to bottom  
 are 320-180, 450-320, 600-450, and 800-600 hPa. Inset boxes give the number of filled 1° × 1° grids. Boundary layer (below 800 hPa)  
 275 data are in Fig. 2.

270 Throughout the free troposphere in all seasons (Fig. 1), cloud-sliced NO<sub>2</sub> is typically 20-60 pptv. In the upper troposphere,  
 lightning NO<sub>x</sub> emissions and photolysis of NO<sub>x</sub> reservoir compounds sustains NO<sub>2</sub> concentrations of 20-70 pptv over the  
 oceans and > 90 pptv over the continents in JJA at 450-320 hPa. NO<sub>2</sub> concentrations exceeding 70 pptv in JJA at 450-320 hPa  
 over North America, China and the Indian subcontinent is due to a combination of lightning and convective uplift of surface  
 anthropogenic pollution (Bertram et al., 2007; Hudman et al., 2007). NO<sub>2</sub> persists for longer in the cold, dry upper troposphere  
 275 (Ehhalt et al., 1992; Jaeglé et al., 1998; Grewe et al., 2001) than in the mid-troposphere below, so NO<sub>2</sub> concentrations are 20



pptv more over Europe and North America at 450-320 hPa than at 600-450 hPa. NO<sub>2</sub> over the open oceans is similar (25-50 pptv) throughout the free troposphere and is due mostly to lightning and continental outflow (Kawakami et al., 1997; Zien et al., 2014). NO<sub>2</sub> in excess of 55 pptv over South America and 80 pptv over Central Africa at 800-600 hPa results from a mix of intense continental lightning and seasonal open burning of biomass (Andreae et al., 2001; Christian et al., 2003; Duncan et al., 2003). The burning season in South America starts in July and occurs throughout JJA in southern Africa and throughout DJF in Africa north of the tropics (Van Der Werf et al., 2006; Castellanos et al., 2014; Van Der Velde et al., 2021). NO<sub>2</sub> is longer-lived in winter, due to cold conditions and slow photolysis (Dickerson et al., 1982; Kenagy et al., 2018), so over continental Europe large surface sources of anthropogenic NO<sub>x</sub> and limited lightning activity especially in comparison to the US contribute to 80 pptv more NO<sub>2</sub> in DJF than in JJA at 800-600 hPa.

285

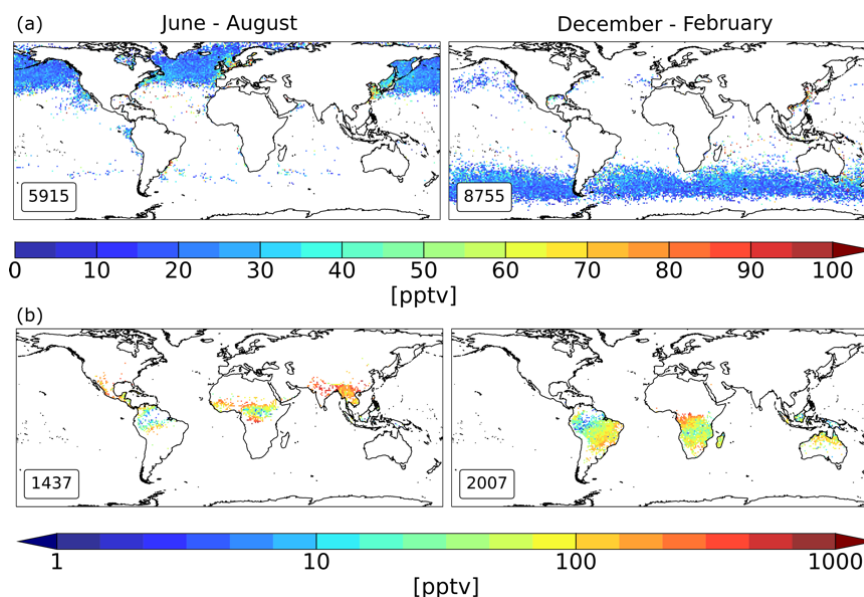


**Figure 2:** As in Fig. 1, but for the boundary layer (below 800 hPa). Panels are NO<sub>2</sub> from cloud-slicing over the oceans (a) and from the differencing approach over land (b) (see Sect. 2.1 for details). Note colourbar ranges differ in panels (a) and (b), and (b) is on a log scale.

290

In the marine boundary layer (Fig. 2 (a)), the typical range in NO<sub>2</sub> concentrations is similar to the layers above, except close to coastlines influenced by continental outflow of anthropogenic pollution and local NO<sub>x</sub> production from busy harbours. Along the east coast of China, for example, NO<sub>2</sub> concentrations are > 90 pptv compared to 25-35 pptv over the remote ocean east of China. In the terrestrial boundary layer (Fig. 2 (b)), NO<sub>2</sub> concentrations exceed 30 pptv and peak at 600 pptv over eastern Brazil in DJF, Central Africa in both seasons and Southeast Asia and the Indo-Gangetic Plain (IGP) in JJA. The peaks in Brazil and Central Africa are due to biomass burning, whereas the peaks in Southeast Asia and the IGP are associated with large urban and industrial sources (Giglio et al., 2010; Ghude et al., 2013; Lu et al., 2024). Steep latitudinal gradients in NO<sub>2</sub> of > 100 pptv obtained with the differencing approach for NO<sub>2</sub> covering Amazonia and Central Africa is due to influence of

295



intense seasonal burning of savanna-type vegetation bordering dense tropical forests (Chen et al., 2013; Osohou et al., 2019;  
300 Jin et al., 2021; Van Der Velde et al., 2021).

The seasonal mean cloud-sliced  $\text{NO}_2$  at 450-180 hPa obtained by Marais et al. (2021) that we compare to our data for the same  
vertical extent and time period (Sect. 2.1) ranges from  $\text{NO}_2 > 80$  pptv over terrestrial regions to  $< 50$  pptv over remote oceans.  
The two datasets are spatially consistent in all seasons, yielding Pearson's correlation coefficients (R) of 0.74 in JJA, 0.70 in  
305 SON, 0.64 in DJF and 0.65 in MAM. Marais et al. (2021)  $\text{NO}_2$  is on average 26% more than we obtain with our updated cloud  
slicing. This difference, decomposed into variance and background using RMA regression, is 25-37% more variance and 17-  
22 pptv less background  $\text{NO}_2$  in our data across all four seasons. The greater background values in Marais et al. (2021) are  
from susceptibility of their approach to outliers (Sect. 2.1).

310 We also examine the size of interannual variability (IAV) in tropospheric  $\text{NO}_2$ , according to our cloud-sliced data. This is  
shown in Fig. 3 for JJA and DJF for a select year (2021 for JJA, December 2020 to February 2021 for DJF), calculated as the  
absolute difference between cloud-sliced  $\text{NO}_2$  in these years and the multiyear mean (Fig. 1). Only three of the five layers are  
shown, as coverage is poor for individual years for the other two layers. IAV data are obtained for  $< 1\%$  of all  $1^\circ \times 1^\circ$  grid cells  
at 180-320 hPa and just 2% in the boundary layer. IAV in the layers shown in Fig. 3 is typically  $\sim 10$  pptv over the remote  
315 ocean and  $\sim 25$  pptv over continental regions (eastern US, Europe, tropics). The greater IAV over the continents is due to  
influence of anthropogenic, open biomass burning and lightning  $\text{NO}_x$  emissions. IAV  $\text{NO}_2$  is about 20-50% of the variability  
the multiyear means in Fig. 1 and 2. Relatively large IAV  $\text{NO}_2$  over the remote oceans is restricted to the edges of sampled  
areas in the subtropics that have low data density, due to the proximity to regions of persistent subsidence where retrievals  
from cloud-slicing are not always successful.

320

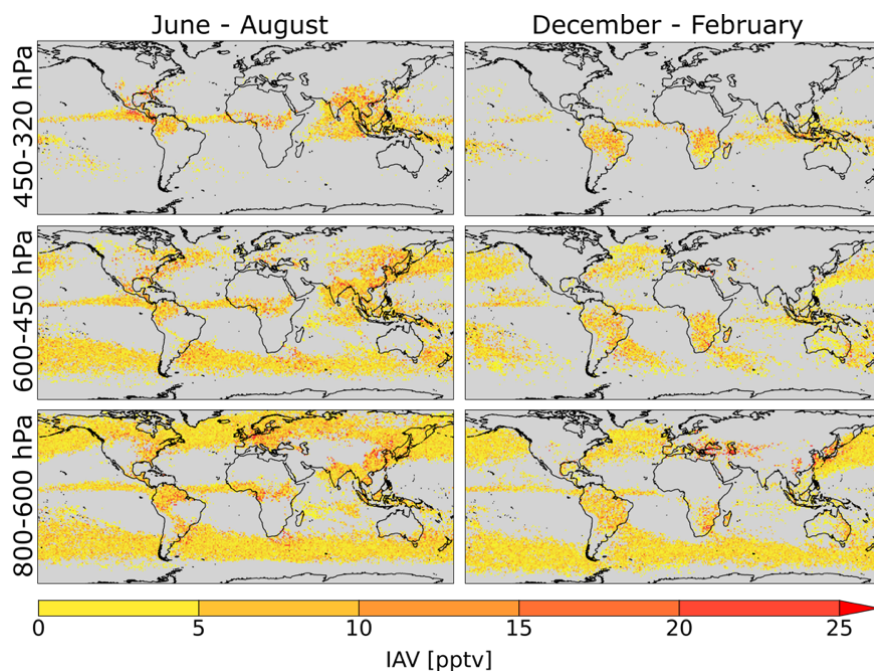


**Figure 3: Free tropospheric NO<sub>2</sub> interannual variability (IAV).** Panels are single-year NO<sub>2</sub> IAV obtained as the absolute difference between single-year (left: JJA 2021; right: DJF 2020-2021) and multiyear mean cloud-sliced NO<sub>2</sub> for the 3 layers with greatest geographic coverage. Only grid squares with at least 5 cloud-sliced data points in the single-year means are compared.

325

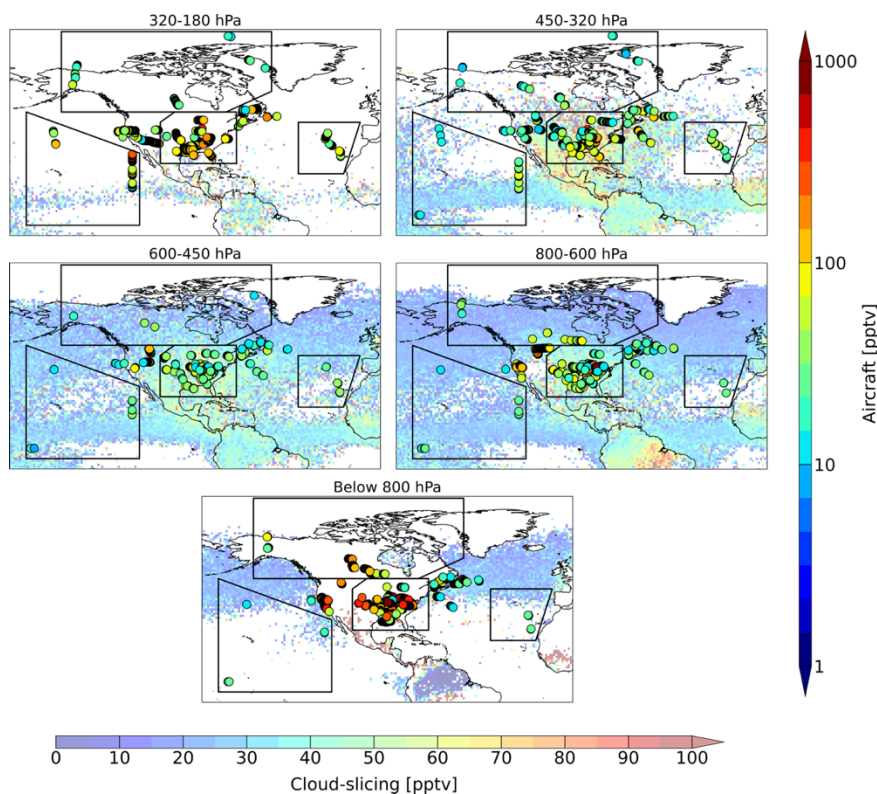
### 3.2 Evaluation of cloud-sliced NO<sub>2</sub> with observed and calculated (PSS) NO<sub>2</sub>

Fig. 4 shows the regions selected to intercompare cloud-sliced and DC-8 NO<sub>2</sub> obtained with direct measurements and PSS NO<sub>2</sub> (Section 2.2). Selected regions include the North Atlantic Ocean sampled during ATom, the Canadian Arctic sampled during ARCTAS and ATom, the eastern United States sampled during SEAC<sup>4</sup>RS and INTEX-A, and the Pacific Ocean sampled during ATom. These regions were chosen to optimise coincidence of aircraft data in all five layers. In many instances, though, coincidence is over a limited extent of the sampling domain, especially the Pacific Ocean in all layers. Domains sampled in all seasons due to the ATom campaign include the Canadian Arctic and the Pacific and Atlantic Oceans. The most sampled time period is JJA, the greatest regional coverage is over the eastern US, and the mid-tropospheric layers (800-600 and 600-450 hPa) have the most DC-8 data. According to the DC-8 NO<sub>2</sub> data, hotspots (NO<sub>2</sub> > 200 pptv) occur over the US terrestrial boundary layer where there are large surface NO<sub>x</sub> emissions. Much lower concentrations of < 25 pptv over the remote ocean are due to absence of large local sources.

330

335





340

**Figure 4: Maps of tropospheric NO<sub>2</sub> over the north-western hemisphere in June-August for the five cloud-slicing pressure ranges. Filled circles are DC-8 NO<sub>2</sub> data along DC-8 flight tracks (Sect. 2.2). Background values are cloud-sliced NO<sub>2</sub>. Polygons show the regions sampled for comparison of aircraft and cloud-sliced NO<sub>2</sub> in Fig. 4 and 5. These are the North Atlantic, the Canadian Arctic, the eastern United States and the Pacific.**

345

Fig. 5 and 6 compare median DC-8 and cloud-sliced NO<sub>2</sub> concentrations in MAM and JJA (Fig. 5) and SON and DJF (Fig. 6) for the polygons in Fig. 4. Cloud-slicing data are for 2018-2021 in JJA and SON, 2018-2022 in DJF, and 2019-2022 in MAM. JJA data are compared to the ARCTAS, SEAC<sup>4</sup>RS, INTEX-A and ATom-1 campaigns, DJF to ATom-2, SON to ATom-3 and SEAC<sup>4</sup>RS, and MAM to ATom-4 and ARCTAS. Vertical profiles of DC-8 NO<sub>2</sub> are relatively stable (~25-50 pptv) throughout the troposphere over Pacific and North Atlantic Oceans and increase exponentially to ~75-300 pptv in the boundary layer over the eastern US and the Canadian Arctic. Most cloud-sliced NO<sub>2</sub> in the mid-troposphere and in the 320-450 hPa layer in the upper troposphere are < 10 pptv different to DC-8 NO<sub>2</sub> in the extensively sampled eastern US and < 25 pptv in the other locations for medians obtained with more than 5 data points. The greater variability in the DC-8 data in each layer (larger interquartile ranges), is because DC-8 are single year measurements, whereas cloud-sliced NO<sub>2</sub> are multiyear means.

355

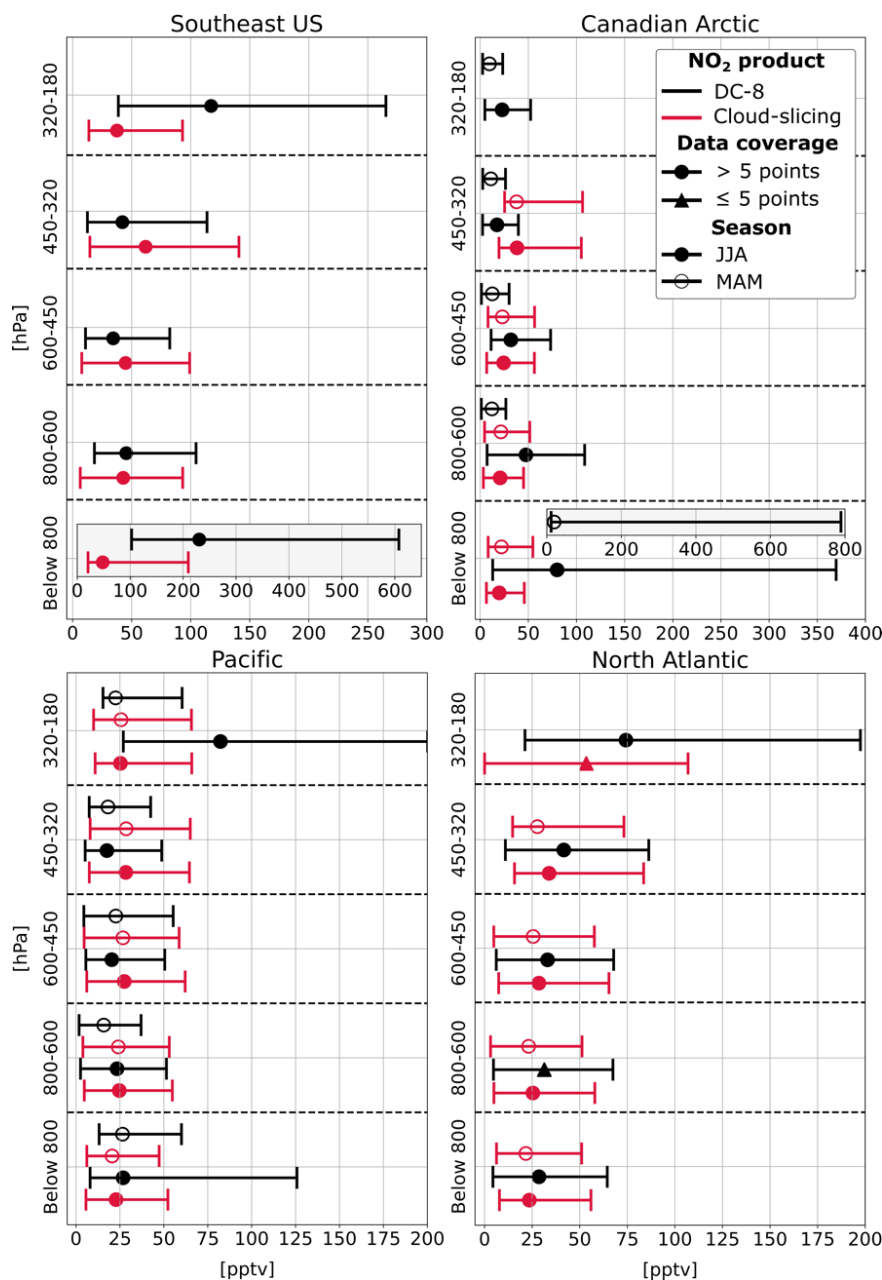


**Figure 5: Comparison of seasonal mean vertical profiles of DC-8 and cloud-sliced tropospheric NO<sub>2</sub>.** Symbols are median values for the sampling domains in Fig. 3 for data in MAM (open) and JJA (filled). Symbol shapes differentiate medians obtained with  $\leq 5$  (triangle) and  $> 5$  (circle) data points in either dataset. Error bars are interquartile ranges (IQR). NO<sub>2</sub> concentration scales differ and inset boxes in the top row show boundary-layer NO<sub>2</sub> exceeding the x-axis range.

360

Large differences between DC-8 and cloud-sliced NO<sub>2</sub> occur in the boundary layer and the top tropospheric layer. In these layers, there are few coincident data points. Most DC-8 data are over land influenced by ground-based sources like intense biomass burning in the boundary layer (Alvarado et al., 2010; Bian et al., 2013) and lightning and convective uplift of surface

365





pollution in the upper troposphere, whereas most cloud-sliced NO<sub>2</sub> in these 2 layers are over the ocean (Fig. 4). The cluster of points in the boundary layer over New England in the northeast US in Fig. 4 have similar coverage from both datasets. These are on median 30 pptv (IQR: 20-50 pptv) for DC-8 and 25 pptv (IQR: 20-30 pptv) for cloud-sliced NO<sub>2</sub>. New England is not included in our comparison in Fig. 5 and 6, as sampling over this location is limited to JJA during INTEX-A.

370

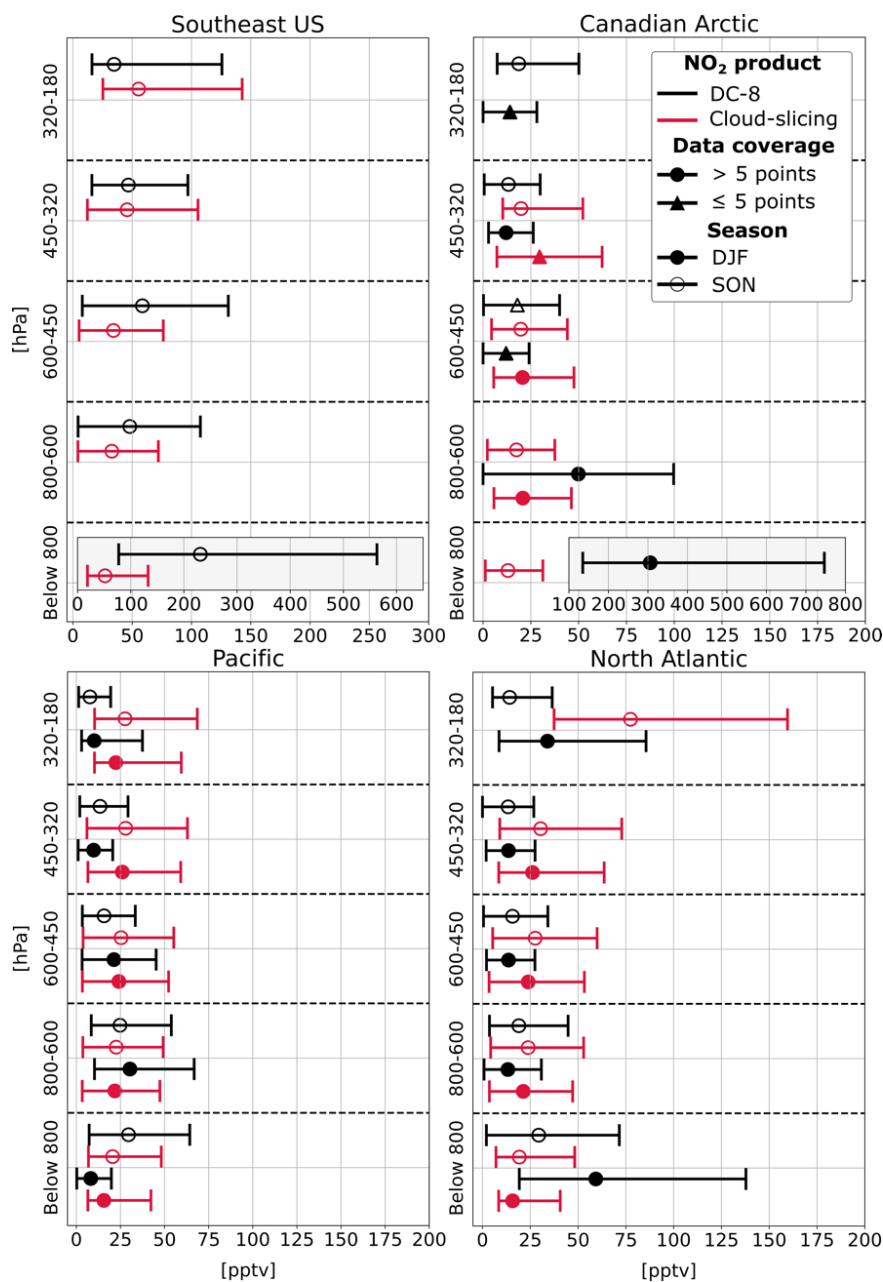
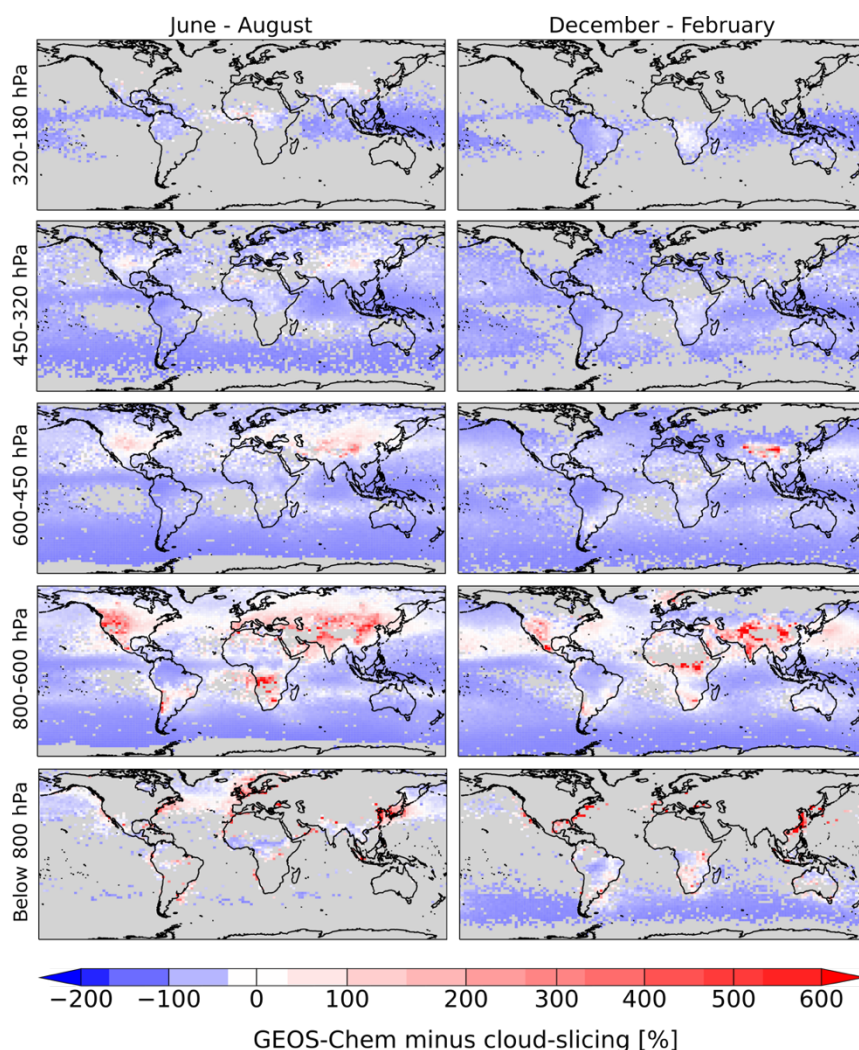


Figure 6: As in Fig. 4, but for SON (open symbols) and DJF (filled symbols).



### 3.3 Comparison of cloud-sliced vertical profiles to synthetic GEOS-Chem profiles

375 Fig. 7 shows the percent difference between multiyear mean GEOS-Chem and cloud-sliced NO<sub>2</sub> for June-August and  
December-February obtained after regridding the cloud-sliced NO<sub>2</sub> to the GEOS-Chem 2° × 2.5° grid. Multiyear means in  
both datasets are compared to minimise influence of interannual variability quantified in Section 3.1. In general, GEOS-Chem  
NO<sub>2</sub> is 30-80% (10-25 pptv) less than cloud-sliced NO<sub>2</sub> in remote locations. Specifically, the Southern Ocean in all layers  
retrieved, South America throughout the free troposphere, and all grid cells except those over Africa in the upper troposphere.  
380 Similar spatial patterns and magnitudes of discrepancies to those plotted in Fig. 7 occur in March-May and September-  
November.





385 **Figure 7: Percent difference between cloud-sliced and GEOS-Chem vertical profiles of tropospheric NO<sub>2</sub>. Maps are at 2° × 2.5°. Blue (red) indicates the model is less (more) than the cloud-sliced NO<sub>2</sub>. Percent difference is calculated as ((GEOS-Chem minus cloud-sliced)/cloud-sliced) for all cloud-sliced 1° × 1° grid squares filled in each year sampled.**

Inclusion of nitrate photolysis in GEOS-Chem decreases the model underestimate in NO<sub>2</sub> over remote regions from 40-80 pptv  
390 to on average ~15 pptv in the mid-troposphere. A relatively large model underestimate of 25-40 pptv over oceans may be due  
to uncertainties in the enhancement factor used to parameterize nitrate photolysis (Section 2.3) (Shah et al., 2023). PPN  
photolysis is most effective at increasing NO<sub>2</sub> in the 2 layers in the upper troposphere where it is abundant and thermally stable,  
so photolysis dominates its conversion to NO<sub>2</sub>. In JJA, for example, PPN photolysis contributes ~65 pptv NO<sub>2</sub> over the northern  
midlatitudes and isolated enhancements of 50-60 pptv over southeast Asia and extending from Mozambique to Madagascar.  
395 As a result of PPN photolysis, the discrepancy between the model and cloud-sliced upper tropospheric NO<sub>2</sub> is relatively small  
(10-30 pptv) over the terrestrial northern midlatitudes. The model exceeds the cloud-sliced data by 20-50 pptv over the northern  
midlatitudes at 600-450 hPa during the summer lightning season north of 35°N. These are the latitudes at which lightning NO<sub>x</sub>  
production rates in GEOS-Chem almost double from 260 moles per flash (mol fl<sup>-1</sup>) to the south to 500 mol fl<sup>-1</sup> to the north  
(Murray et al., 2012). The effect of this on NO<sub>2</sub> is also evident at 450-320 hPa, though the spatial extent and dataset differences  
400 are smaller in this layer. 500 mol fl<sup>-1</sup> prescribed to northern midlatitude lightning far exceeds observationally constrained  
global mean estimates of ~280 mol fl<sup>-1</sup> (Marais et al., 2018) and regional mean estimates of 180 mol fl<sup>-1</sup> for the northern  
midlatitudes (Bucsela et al., 2019) and 230-360 mol fl<sup>-1</sup> for the US and western Atlantic (Allen et al., 2021).

The largest differences between the two datasets occur in the boundary layer along coastlines in North America, Europe and  
405 China influenced by anthropogenic pollution. This may in part be due to the different years targeted. COVID lockdowns  
influenced surface emissions of traffic NO<sub>x</sub> in the cloud-sliced data and anthropogenic NO<sub>x</sub> emissions are steadily declining  
over North America, Europe and China as a result of air quality regulation (Zhao et al., 2013; Lloret and Valiela, 2016; Clappier  
et al., 2021). Both COVID lockdowns and emissions reductions policies would contribute to a model overestimate in NO<sub>2</sub>.  
GEOS-Chem also exceeds cloud-sliced NO<sub>2</sub> at multiple locations in the 800-600 hPa layer. These include southern Africa in  
410 JJA and northern Africa in DJF coincident with the dry burning season of these regions, central Asia in all seasons where there  
are large sources of anthropogenic pollution. The apparent model overestimate over western US at 600-800 hPa occurs in all  
seasons and may result from a combination of factors. The TROPOMI sampling period includes the high-fire year (2020)  
(Albores et al., 2023) and the model does not, affecting the comparison in seasons coincident with the fire season (JJA, SON).  
The number of cloud-sliced data points are also relatively few over this region of subsidence. It is difficult to diagnose  
415 discrepancies in the tropical terrestrial boundary layer, as anthropogenic emissions inventories are prone to misrepresenting  
sources unique to the tropics (Duncan et al., 2003; Marais and Wiedinmyer, 2016; Vohra et al., 2022) and there are no suitable  
independent in-situ measurements to validate the differencing approach we use to derive NO<sub>2</sub>.



#### 4 Conclusions

Global vertical profiles of tropospheric NO<sub>2</sub> were obtained for five discrete layers (180-320 hPa, 320-450 hPa, 450-600 hPa, 600-800 hPa, and below 800 hPa) by cloud-slicing TROPOMI total columns of NO<sub>2</sub> above optically thick clouds. These were assessed against directly measured and calculated (photostationary steady-state) NASA DC-8 aircraft NO<sub>2</sub> measurements from 2004 to 2018. We then applied our cloud-sliced NO<sub>2</sub> to evaluate contemporary understanding of climatological tropospheric NO<sub>x</sub> as simulated by GEOS-Chem. We found that coverage from cloud-slicing is greatest in the mid-troposphere (60-70%) where there is an abundance of optically thick clouds and least (8% coverage, mostly in the tropics) in the upper troposphere. Cloud-sliced NO<sub>2</sub> ranges from < 35 pptv throughout the troposphere over remote marine regions, to 20-60 pptv in the free troposphere over continents, to 160-380 pptv in the boundary layer over source regions in the US, Europe and Asia. Free tropospheric NO<sub>2</sub> exhibits very little interannual variability, ranging from ~10 pptv over oceans to ~25 pptv over land.

We determined from comparison of cloud-sliced NO<sub>2</sub> to NASA DC-8 aircraft observations that cloud-sliced NO<sub>2</sub> differs from DC-8 NO<sub>2</sub> by just 5-10 pptv when sampling in both datasets is abundant and consistent. It was not feasible to assess cloud-sliced NO<sub>2</sub> in the boundary layer and in the highest cloud-sliced layer, due to a lack of sufficient coincident data in the tropics. The GEOS-Chem model that represents contemporary understanding of tropospheric NO<sub>x</sub> simulates NO<sub>2</sub> that is typically 10-40 pptv less than cloud-sliced NO<sub>2</sub> in the remote upper troposphere and over the remote oceans. This is a substantial improvement on the > 40 pptv model underestimate before accounting for NO<sub>x</sub> recycling in the upper troposphere via PPN photolysis and in the middle and lower troposphere via aerosol nitrate photolysis. Differences are greater over source regions influenced by lightning and open burning of biomass and with evolving anthropogenic emissions due to rapid development, policies and events like lockdowns in response to the COVID-19 pandemic. A model high bias of 50 pptv over the northern hemisphere mid-troposphere in June-August points to an issue with the model lightning NO<sub>x</sub> production rates that are almost double production rates everywhere else.

Limited coincident reliable observations to validate cloud-sliced NO<sub>2</sub> remains a challenge, but as we demonstrate cloud-sliced NO<sub>2</sub> hold value for assessing air quality, chemical transport, and Earth System models to identify differences that warrant further investigation, especially given reliance on these models to understand complex tropospheric chemistry, inform policies, and retrieve trace gas abundances from satellites. Geostationary instruments will further enhance the utility of cloud-sliced NO<sub>2</sub> datasets to also investigate daytime variability in vertical profiles of tropospheric NO<sub>x</sub>.



*Data Availability.* The multiyear seasonal mean NO<sub>2</sub> from cloud-slicing TROPOMI and from simulating the GEOS-Chem  
450 model are publicly available from the UCL Data Repository (<https://doi.org/10.5522/04/25782336>).

*Author contributions.* Study concept by EAM and RPH. RPH led the writing and analysis, simulated GEOS-Chem and cloud-  
sliced TROPOMI NO<sub>2</sub> with supervision from EAM. NW provided the NASA DC-8 python processing code. RGR updated the  
GEOS-Chem model to include PPN photolysis. VS updated the GEOS-Chem model to include particulate nitrate photolysis.  
455 All authors reviewed and edited the manuscript.

*Competing interests.* The authors declare that they have no conflict of interest.

*Acknowledgements.* This research has been supported by the European Research Council under the European Union's Horizon  
460 2020 research and innovation programme (through a Starting Grant awarded to Eloise A. Marais, UpTrop [grant no. 851854]).  
We are grateful to NASA DC-8 aircraft campaign teams for access to observations, specifically the NO<sub>2</sub> measurement PIs:  
Ronald Cohen (INTEX-A), Andrew Weinheimer (ARCTAS), Thomas B. Ryerson (SEAC<sup>4</sup>RS), and Chelsea Thompson  
(ATom).



## 465 References

- Albores, I. S., Buchholz, R. R., Ortega, I., Emmons, L. K., Hannigan, J. W., Lacey, F., Pfister, G., Tang, W., and Worden, H. M.: Continental-scale Atmospheric Impacts of the 2020 Western U.S. Wildfires, *Atmos. Environ.*, 294, 119436, <https://doi.org/10.1016/j.atmosenv.2022.119436>, 2023.
- 470 Allen, D. J., Pickering, K. E., Lamsal, L., Mach, D. M., Quick, M. G., Lapierre, J., Janz, S., Koshak, W., Kowalewski, M., and Blakeslee, R.: Observations of Lightning NO<sub>x</sub> Production From GOES-R Post Launch Test Field Campaign Flights, *J. Geophys. Res. Atmospheres*, 126, e2020JD033769, <https://doi.org/10.1029/2020JD033769>, 2021.
- Alvarado, M. J., Logan, J. A., Mao, J., Apel, E., Riemer, D., Blake, D., Cohen, R. C., Min, K.-E., Perring, A. E., Browne, E. C., Wooldridge, P. J., Diskin, G. S., Sachse, G. W., Fuelberg, H., Sessions, W. R., Harrigan, D. L., Huey, G., Liao, J., Case-  
475 Hanks, A., Jimenez, J. L., Cubison, M. J., Vay, S. A., Weinheimer, A. J., Knapp, D. J., Montzka, D. D., Flocke, F. M., Pollack, I. B., Wennberg, P. O., Kurten, A., Crouse, J., Clair, J. M. St., Wisthaler, A., Mikoviny, T., Yantosca, R. M., Carouge, C. C., and Le Sager, P.: Nitrogen oxides and PAN in plumes from boreal fires during ARCTAS-B and their impact on ozone: an integrated analysis of aircraft and satellite observations, *Atmospheric Chem. Phys.*, 10, 9739–9760, <https://doi.org/10.5194/acp-10-9739-2010>, 2010.
- 480 Andersen, S. T., Carpenter, L. J., Reed, C., Lee, J. D., Chance, R., Sherwen, T., Vaughan, A. R., Stewart, J., Edwards, P. M., Bloss, W. J., Sommariva, R., Crilley, L. R., Nott, G. J., Neves, L., Read, K., Heard, D. E., Seakins, P. W., Whalley, L. K., Boustead, G. A., Fleming, L. T., Stone, D., and Fomba, K. W.: Extensive field evidence for the release of HONO from the photolysis of nitrate aerosols, *Sci. Adv.*, 9, <https://doi.org/10.1126/sciadv.add6266>, 2023.
- Andreae, M. O., Artaxo, P., Fischer, H., Freitas, S. R., Grégoire, J.-M., Hansel, A., Hoor, P., Kormann, R., Krejci, R., Lange,  
485 L., Lelieveld, J., Lindinger, W., Longo, K., Peters, W., De Reus, M., Scheeren, B., Silva Dias, M. A. F., Ström, J., Van Velthoven, P. F. J., and Williams, J.: Transport of biomass burning smoke to the upper troposphere by deep convection in the equatorial region, *Geophys. Res. Lett.*, 28, 951–954, <https://doi.org/10.1029/2000GL012391>, 2001.
- ARCTAS Science Team: Arctic Research of the Composition of the Troposphere from Aircraft and Satellites (ARCTAS) NASA Airborne Mission Overview, <https://doi.org/10.5067/SUBORBITAL/ARCTAS2008/DATA001>, 2011.
- 490 Atkinson, R.: Atmospheric chemistry of VOCs and NO<sub>x</sub>, *Atmos. Environ.*, 34, 2063–2101, [https://doi.org/10.1016/S1352-2310\(99\)00460-4](https://doi.org/10.1016/S1352-2310(99)00460-4), 2000.
- ATom Science Team: Atmospheric Tomography Mission (ATom): Merged Atmospheric Chemistry, Trace Gases, and Aerosols, Version 2, <https://doi.org/10.3334/ORNLDAAAC/1925>, 2021.
- Barth, M. C., Cantrell, C. A., Brune, W. H., Rutledge, S. A., Crawford, J. H., Huntrieser, H., Carey, L. D., MacGorman, D.,  
495 Weisman, M., Pickering, K. E., Bruning, E., Anderson, B., Apel, E., Biggerstaff, M., Campos, T., Campuzano-Jost, P., Cohen, R., Crouse, J., Day, D. A., Diskin, G., Flocke, F., Fried, A., Garland, C., Heikes, B., Honomichl, S., Hornbrook, R., Huey, L. G., Jimenez, J. L., Lang, T., Lichtenstern, M., Mikoviny, T., Nault, B., O’Sullivan, D., Pan, L. L., Peischl, J., Pollack, I., Richter, D., Riemer, D., Ryerson, T., Schlager, H., St. Clair, J., Walega, J., Weibring, P., Weinheimer, A., Wennberg, P., Wisthaler, A., Wooldridge, P. J., and Ziegler, C.: The Deep Convective Clouds and Chemistry (DC3) Field Campaign, *Bull.*  
500 *Am. Meteorol. Soc.*, 96, 1281–1309, <https://doi.org/10.1175/BAMS-D-13-00290.1>, 2015.
- Belmonte Rivas, M., Veeffkind, P., Eskes, H., and Levelt, P.: OMI tropospheric NO<sub>2</sub> profiles from cloud slicing: constraints on surface emissions, convective transport and lightning NO<sub>x</sub>, *Atmospheric Chem. Phys. Discuss.*, 15, 8017–8072, <https://doi.org/10.5194/acpd-15-8017-2015>, 2015.





- 505 Bertram, T. H., Perring, A. E., Wooldridge, P. J., Crounse, J. D., Kwan, A. J., Wennberg, P. O., Scheuer, E., Dibb, J., Avery, M., Sachse, G., Vay, S. A., Crawford, J. H., McNaughton, C. S., Clarke, A., Pickering, K. E., Fuelberg, H., Huey, G., Blake, D. R., Singh, H. B., Hall, S. R., Shetter, R. E., Fried, A., Heikes, B. G., and Cohen, R. C.: Direct Measurements of the Convective Recycling of the Upper Troposphere, *Science*, 315, 816–820, <https://doi.org/10.1126/science.1134548>, 2007.
- 510 Bian, H., Colarco, P. R., Chin, M., Chen, G., Rodriguez, J. M., Liang, Q., Blake, D., Chu, D. A., Da Silva, A., Darmenov, A. S., Diskin, G., Fuelberg, H. E., Huey, G., Kondo, Y., Nielsen, J. E., Pan, X., and Wisthaler, A.: Source attributions of pollution to the Western Arctic during the NASA ARCTAS field campaign, *Atmospheric Chem. Phys.*, 13, 4707–4721, <https://doi.org/10.5194/acp-13-4707-2013>, 2013.
- Bloss, W. J., Evans, M. J., Lee, J. D., Sommariva, R., Heard, D. E., and Pilling, M. J.: The oxidative capacity of the troposphere: Coupling of field measurements of OH and a global chemistry transport model, *Faraday Discuss.*, 130, 425, <https://doi.org/10.1039/b419090d>, 2005.
- 515 Boersma, K. F., Eskes, H. J., and Brinksma, E. J.: Error analysis for tropospheric NO<sub>2</sub> retrieval from space, *J. Geophys. Res. Atmospheres*, 109, <https://doi.org/10.1029/2003JD003962>, 2004.
- Bradshaw, J., Davis, D., Grodzinsky, G., Smyth, S., Newell, R., Sandholm, S., and Liu, S.: Observed distributions of nitrogen oxides in the remote free troposphere from the Nasa Global Tropospheric Experiment Programs, *Rev. Geophys.*, 38, 61–116, <https://doi.org/10.1029/1999RG900015>, 2000.
- 520 Brenninkmeijer, C. A. M., Crutzen, P. J., Fischer, H., Güsten, H., Hans, W., Heinrich, G., Heintzenberg, J., Hermann, M., Immelmann, T., Kersting, D., Maiss, M., Nolle, M., Pitscheider, A., Pohlkamp, H., Scharffe, D., Specht, K., and Wiedensohler, A.: CARIBIC—Civil Aircraft for Global Measurement of Trace Gases and Aerosols in the Tropopause Region, *J. Atmospheric Ocean. Technol.*, 16, 1373–1383, [https://doi.org/10.1175/1520-0426\(1999\)016<1373:CCAFGM>2.0.CO;2](https://doi.org/10.1175/1520-0426(1999)016<1373:CCAFGM>2.0.CO;2), 1999.
- 525 Browne, E. C., Perring, A. E., Wooldridge, P. J., Apel, E., Hall, S. R., Huey, L. G., Mao, J., Spencer, K. M., Clair, J. M. St., Weinheimer, A. J., Wisthaler, A., and Cohen, R. C.: Global and regional effects of the photochemistry of CH<sub>3</sub>O<sub>2</sub>NO<sub>2</sub> evidence from ARCTAS, *Atmospheric Chem. Phys.*, 11, 4209–4219, <https://doi.org/10.5194/acp-11-4209-2011>, 2011.
- Bucsela, E. J., Pickering, K. E., Allen, D. J., Holzworth, R. H., and Krotkov, N. A.: Midlatitude Lightning NO<sub>x</sub> Production Efficiency Inferred From OMI and WLLN Data, *J. Geophys. Res. Atmospheres*, 124, 13475–13497, <https://doi.org/10.1029/2019JD030561>, 2019.
- 530 Burkholder, J. B., Sander, S. P., Abbatt, J. P. D., Barker, J. R., Cappa, C., Crounse, J. D., Dibble, T. S., Huie, R. E., Kolb, C. E., Kurylo, M. J., Orkin, V. L., Percival, C. J., Wilmouth, D. M., and Wine, P. H.: Chemical Kinetics and Photochemical Data for Use in Atmospheric Studies, Evaluation No. 19, 2020.
- 535 Castellanos, P., Boersma, K. F., and Van Der Werf, G. R.: Satellite observations indicate substantial spatiotemporal variability in biomass burning NO<sub>x</sub> emission factors for South America, *Atmospheric Chem. Phys.*, 14, 3929–3943, <https://doi.org/10.5194/acp-14-3929-2014>, 2014.
- Chatfield, R. B.: Anomalous HNO<sub>3</sub>/NO<sub>x</sub> ratio of remote tropospheric air: Conversion of nitric acid to formic acid and NO<sub>x</sub>?, *Geophys. Res. Lett.*, 21, 2705–2708, <https://doi.org/10.1029/94GL02659>, 1994.
- 540 Chen, Y., Morton, D. C., Jin, Y., Collatz, G. J., Kasibhatla, P. S., Van Der Werf, G. R., DeFries, R. S., and Randerson, J. T.: Long-term trends and interannual variability of forest, savanna and agricultural fires in South America, *Carbon Manag.*, 4, 617–638, <https://doi.org/10.4155/cmt.13.61>, 2013.



- Choi, S., Joiner, J., Choi, Y., Duncan, B. N., Vasilkov, A., Krotkov, N., and Bucsela, E.: First estimates of global free-tropospheric NO<sub>2</sub> abundances derived using a cloud-slicing technique applied to satellite observations from the Aura Ozone Monitoring Instrument (OMI), *Atmospheric Chem. Phys.*, 14, 10565–10588, <https://doi.org/10.5194/acp-14-10565-2014>, 2014.
- 545 Christian, H. J., Blakeslee, R. J., Boccippio, D. J., Boeck, W. L., Buechler, D. E., Driscoll, K. T., Goodman, S. J., Hall, J. M., Koshak, W. J., Mach, D. M., and Stewart, M. F.: Global frequency and distribution of lightning as observed from space by the Optical Transient Detector, *J. Geophys. Res. Atmospheres*, 108, <https://doi.org/10.1029/2002JD002347>, 2003.
- Clappier, A., Thunis, P., Beekmann, M., Putaud, J. P., and De Meij, A.: Impact of SO<sub>x</sub>, NO<sub>x</sub> and NH<sub>3</sub> emission reductions on PM<sub>2.5</sub> concentrations across Europe: Hints for future measure development, *Environ. Int.*, 156, 106699, <https://doi.org/10.1016/j.envint.2021.106699>, 2021.
- 560 Crawford, J., Davis, D., Chen, G., Bradshaw, J., Sandholm, S., Gregory, G., Sachse, G., Anderson, B., Collins, J., Blake, D., Singh, H., Heikes, B., Talbot, R., and Rodriguez, J.: Photostationary state analysis of the NO<sub>2</sub>-NO system based on airborne observations from the western and central North Pacific, *J. Geophys. Res. Atmospheres*, 101, 2053–2072, <https://doi.org/10.1029/95JD02201>, 1996.
- 555 Crutzen, P. J. and Andreae, M. O.: Biomass Burning in the Tropics: Impact on Atmospheric Chemistry and Biogeochemical Cycles, *Science*, 250, 1669–1678, <https://doi.org/10.1126/science.250.4988.1669>, 1990.
- Davis, D. D., Chen, G., Chameides, W., Bradshaw, J., Sandholm, S., Rodgers, M., Schendal, J., Madronich, S., Sachse, G., Gregory, G., Anderson, B., Barrick, J., Shipham, M., Collins, J., Wade, L., and Blake, D.: A photostationary state analysis of the NO<sub>2</sub>-NO system based on airborne observations from the subtropical/tropical North and South Atlantic, *J. Geophys. Res.*, 98, 23501, <https://doi.org/10.1029/93JD02412>, 1993.
- 560 Di Carlo, P., Aruffo, E., Busilacchio, M., Giammaria, F., Dari-Salisburgo, C., Biancofiore, F., Visconti, G., Lee, J., Moller, S., Reeves, C. E., Bauguitte, S., Forster, G., Jones, R. L., and Ouyang, B.: Aircraft based four-channel thermal dissociation laser induced fluorescence instrument for simultaneous measurements of NO<sub>2</sub>, total peroxy nitrate, total alkyl nitrate, and HNO<sub>3</sub>, *Atmospheric Meas. Tech.*, 6, 971–980, <https://doi.org/10.5194/amt-6-971-2013>, 2013.
- 565 Dickerson, R. R., Stedman, D. H., and Delany, A. C.: Direct measurements of ozone and nitrogen dioxide photolysis rates in the troposphere, *J. Geophys. Res. Oceans*, 87, 4933–4946, <https://doi.org/10.1029/JC087iC07p04933>, 1982.
- Dignon, J.: NO<sub>x</sub> and SO<sub>x</sub> emissions from fossil fuels: A global distribution, *Atmospheric Environ. Part Gen. Top.*, 26, 1157–1163, [https://doi.org/10.1016/0960-1686\(92\)90047-O](https://doi.org/10.1016/0960-1686(92)90047-O), 1992.
- 570 Duncan, B. N., Martin, R. V., Staudt, A. C., Yevich, R., and Logan, J. A.: Interannual and seasonal variability of biomass burning emissions constrained by satellite observations, *J. Geophys. Res.*, 108, 4100, <https://doi.org/10.1029/2002JD002378>, 2003.
- Ehnhalt, D. H., Rohrer, F., and Wahner, A.: Sources and distribution of NO<sub>x</sub> in the upper troposphere at northern mid-latitudes, *J. Geophys. Res.*, 97, 3725, <https://doi.org/10.1029/91JD03081>, 1992.
- 575 Emmons, L. K., Hauglustaine, D. A., Müller, J., Carroll, M. A., Brasseur, G. P., Brunner, D., Staehelin, J., Thouret, V., and Marenco, A.: Data composites of airborne observations of tropospheric ozone and its precursors, *J. Geophys. Res. Atmospheres*, 105, 20497–20538, <https://doi.org/10.1029/2000JD900232>, 2000.
- Eskes, H. J. and Eichmann, K.-U.: S5P Mission Performance Centre Nitrogen Dioxide [L2\_\_NO2\_\_] Readme, 2023.



- 580 Fuelberg, H. E., Hannan, J. R., Van Velthoven, P. F. J., Browell, E. V., Bieberbach, G., Knabb, R. D., Gregory, G. L., Pickering, K. E., and Selkirk, H. B.: A meteorological overview of the Subsonic Assessment Ozone and Nitrogen Oxide Experiment (SONEX) period, *J. Geophys. Res. Atmospheres*, 105, 3633–3651, <https://doi.org/10.1029/1999JD900917>, 2000.
- Ghude, S. D., Kulkarni, S. H., Jena, C., Pfister, G. G., Beig, G., Fadnavis, S., and Van Der A, R. J.: Application of satellite observations for identifying regions of dominant sources of nitrogen oxides over the Indian Subcontinent, *J. Geophys. Res. Atmospheres*, 118, 1075–1089, <https://doi.org/10.1029/2012JD017811>, 2013.
- 585 Giglio, L., Randerson, J. T., Van Der Werf, G. R., Kasibhatla, P. S., Collatz, G. J., Morton, D. C., and DeFries, R. S.: Assessing variability and long-term trends in burned area by merging multiple satellite fire products, *Biogeosciences*, 7, 1171–1186, <https://doi.org/10.5194/bg-7-1171-2010>, 2010.
- Grewe, V., Brunner, D., Dameris, M., Grenfell, J. L., Hein, R., Shindell, D., and Staehelin, J.: Origin and variability of upper tropospheric nitrogen oxides and ozone at northern mid-latitudes, *Atmos. Environ.*, 35, 3421–3433, [https://doi.org/10.1016/S1352-2310\(01\)00134-0](https://doi.org/10.1016/S1352-2310(01)00134-0), 2001.
- 590 Guo, H., Flynn, C. M., Prather, M. J., Strode, S. A., Steenrod, S. D., Emmons, L., Lacey, F., Lamarque, J.-F., Fiore, A. M., Correa, G., Murray, L. T., Wolfe, G. M., St. Clair, J. M., Kim, M., Crounse, J., Diskin, G., DiGangi, J., Daube, B. C., Commane, R., McKain, K., Peischl, J., Ryerson, T. B., Thompson, C., Hanisco, T. F., Blake, D., Blake, N. J., Apel, E. C., Hornbrook, R. S., Elkins, J. W., Hints, E. J., Moore, F. L., and Wofsy, S. C.: Heterogeneity and chemical reactivity of the remote troposphere defined by aircraft measurements, *Atmospheric Chem. Phys.*, 23, 99–117, <https://doi.org/10.5194/acp-23-99-2023>, 2023.
- 595 Harwood, M. H., Roberts, J. M., Frost, G. J., Ravishankara, A. R., and Burkholder, J. B.: Photochemical Studies of  $\text{CH}_3\text{C}(\text{O})\text{OONO}_2$  (PAN) and  $\text{CH}_3\text{CH}_2\text{C}(\text{O})\text{OONO}_2$  (PPN):  $\text{NO}_3$  Quantum Yields, *J. Phys. Chem. A*, 107, 1148–1154, <https://doi.org/10.1021/jp0264230>, 2003.
- 600 Hudman, R. C., Jacob, D. J., Turquety, S., Leibensperger, E. M., Murray, L. T., Wu, S., Gilliland, A. B., Avery, M., Bertram, T. H., Brune, W., Cohen, R. C., Dibb, J. E., Flocke, F. M., Fried, A., Holloway, J., Neuman, J. A., Orville, R., Perring, A., Ren, X., Sachse, G. W., Singh, H. B., Swanson, A., and Wooldridge, P. J.: Surface and lightning sources of nitrogen oxides over the United States: Magnitudes, chemical evolution, and outflow, *J. Geophys. Res. Atmospheres*, 112, 2006JD007912, <https://doi.org/10.1029/2006JD007912>, 2007.
- 605 Jacob, D. J., Crawford, J. H., Maring, H., Clarke, A. D., Dibb, J. E., Emmons, L. K., Ferrare, R. A., Hostetler, C. A., Russell, P. B., Singh, H. B., Thompson, A. M., Shaw, G. E., McCauley, E., Pederson, J. R., and Fisher, J. A.: The Arctic Research of the Composition of the Troposphere from Aircraft and Satellites (ARCTAS) mission: design, execution, and first results, *Atmospheric Chem. Phys.*, 10, 5191–5212, <https://doi.org/10.5194/acp-10-5191-2010>, 2010.
- Jaeglé, L., Jacob, D. J., Wang, Y., Weinheimer, A. J., Ridley, B. A., Campos, T. L., Sachse, G. W., and Hagen, D. E.: Sources and chemistry of  $\text{NO}_x$  in the upper troposphere over the United States, *Geophys. Res. Lett.*, 25, 1705–1708, <https://doi.org/10.1029/97GL03591>, 1998.
- 610 Jain, A. K., Tao, Z., Yang, X., and Gillespie, C.: Estimates of global biomass burning emissions for reactive greenhouse gases ( $\text{CO}$ , NMHCs, and  $\text{NO}_x$ ) and  $\text{CO}_2$ , *J. Geophys. Res.*, 111, D06304, <https://doi.org/10.1029/2005JD006237>, 2006.
- Jin, X., Zhu, Q., and Cohen, R. C.: Direct estimates of biomass burning  $\text{NO}_x$  emissions and lifetimes using daily observations from TROPOMI, *Atmospheric Chem. Phys.*, 21, 15569–15587, <https://doi.org/10.5194/acp-21-15569-2021>, 2021.
- 615 Kang, Y., Tang, G., Li, Q., Liu, B., Cao, J., Hu, Q., and Wang, Y.: Evaluation and Evolution of MAX-DOAS-observed Vertical  $\text{NO}_2$  Profiles in Urban Beijing, *Adv. Atmospheric Sci.*, 38, 1188–1196, <https://doi.org/10.1007/s00376-021-0370-1>, 2021.



- Karl, T. G., Christian, T. J., Yokelson, R. J., Artaxo, P., Hao, W. M., and Guenther, A.: The Tropical Forest and Fire Emissions Experiment: method evaluation of volatile organic compound emissions measured by PTR-MS, FTIR, and GC from tropical biomass burning, *Atmospheric Chem. Phys.*, 7, 5883–5897, <https://doi.org/10.5194/acp-7-5883-2007>, 2007.
- 620 Kasibhatla, P., Sherwen, T., Evans, M. J., Carpenter, L. J., Reed, C., Alexander, B., Chen, Q., Sulprizio, M. P., Lee, J. D., Read, K. A., Bloss, W., Crilley, L. R., Keene, W. C., Pszenny, A. A. P., and Hodzic, A.: Global impact of nitrate photolysis in sea-salt aerosol on NO<sub>x</sub>, OH, and O<sub>3</sub> in the marine boundary layer, *Atmospheric Chem. Phys.*, 18, 11185–11203, <https://doi.org/10.5194/acp-18-11185-2018>, 2018.
- 625 Kawakami, S., Kondo, Y., Koike, M., Nakajima, H., Gregory, G. L., Sachse, G. W., Newell, R. E., Browell, E. V., Blake, D. R., Rodriguez, J. M., and Merrill, J. T.: Impact of lightning and convection on reactive nitrogen in the tropical free troposphere, *J. Geophys. Res. Atmospheres*, 102, 28367–28384, <https://doi.org/10.1029/97JD02073>, 1997.
- Kenagy, H. S., Sparks, T. L., Ebben, C. J., Wooldrige, P. J., Lopez-Hilfiker, F. D., Lee, B. H., Thornton, J. A., McDuffie, E. E., Fibiger, D. L., Brown, S. S., Montzka, D. D., Weinheimer, A. J., Schroder, J. C., Campuzano-Jost, P., Day, D. A., Jimenez, J. L., Dibb, J. E., Campos, T., Shah, V., Jaeglé, L., and Cohen, R. C.: NO<sub>x</sub> Lifetime and NO<sub>y</sub> Partitioning During WINTER, *J. Geophys. Res. Atmospheres*, 123, 9813–9827, <https://doi.org/10.1029/2018JD028736>, 2018.
- 630 Kotamarthi, V. R., Gaffney, J. S., Marley, N. A., and Doskey, P. V.: Heterogeneous NO<sub>x</sub> chemistry in the polluted PBL, *Atmos. Environ.*, 35, 4489–4498, [https://doi.org/10.1016/S1352-2310\(01\)00221-7](https://doi.org/10.1016/S1352-2310(01)00221-7), 2001.
- Liu, S., Valks, P., Pinardi, G., Xu, J., Chan, K. L., Argyrouli, A., Lutz, R., Beirle, S., Khorsandi, E., Baier, F., Huijnen, V., Bais, A., Donner, S., Dörner, S., Gratsea, M., Hendrick, F., Karagkiozidis, D., Lange, K., PETERS, A. J. M., Remmers, J., Richter, A., Van Roozendaal, M., Wagner, T., Wenig, M., and Loyola, D. G.: An improved TROPOMI tropospheric NO<sub>2</sub> research product over Europe, *Atmospheric Meas. Tech.*, 14, 7297–7327, <https://doi.org/10.5194/amt-14-7297-2021>, 2021.
- 635 Lloret, J. and Valiela, I.: Unprecedented decrease in deposition of nitrogen oxides over North America: the relative effects of emission controls and prevailing air-mass trajectories, *Biogeochemistry*, 129, 165–180, <https://doi.org/10.1007/s10533-016-0225-5>, 2016.
- Loyola, D. G., Gimeno García, S., Lutz, R., Argyrouli, A., Romahn, F., Spurr, R. J. D., Pedernana, M., Doicu, A., Molina García, V., and Schüssler, O.: The operational cloud retrieval algorithms from TROPOMI on board Sentinel-5 Precursor, *Atmospheric Meas. Tech.*, 11, 409–427, <https://doi.org/10.5194/amt-11-409-2018>, 2018.
- 640 Lu, G., Marais, E. A., Vohra, K., Horner, R. P., Zhang, D., Martin, R. V., and Guttikunda, S. K.: Near-Automated Estimate of City Nitrogen Oxides Emissions Applied to South and Southeast Asia, <https://doi.org/10.22541/essoar.171033213.36792308/v1>, 13 March 2024.
- 645 Marais, E. A. and Wiedinmyer, C.: Air Quality Impact of Diffuse and Inefficient Combustion Emissions in Africa (DICE-Africa), *Environ. Sci. Technol.*, 50, 10739–10745, <https://doi.org/10.1021/acs.est.6b02602>, 2016.
- Marais, E. A., Jacob, D. J., Jimenez, J. L., Campuzano-Jost, P., Day, D. A., Hu, W., Krechmer, J., Zhu, L., Kim, P. S., Miller, C. C., Fisher, J. A., Travis, K., Yu, K., Hanisco, T. F., Wolfe, G. M., Arkinson, H. L., Pye, H. O. T., Froyd, K. D., Liao, J., and McNeill, V. F.: Aqueous-phase mechanism for secondary organic aerosol formation from isoprene: application to the southeast United States and co-benefit of SO<sub>2</sub> emission controls, *Atmospheric Chem. Phys.*, 16, 1603–1618, <https://doi.org/10.5194/acp-16-1603-2016>, 2016.
- 650 Marais, E. A., Jacob, D. J., Choi, S., Joiner, J., Belmonte-Rivas, M., Cohen, R. C., Beirle, S., Murray, L. T., Schiferl, L. D., Shah, V., and Jaeglé, L.: Nitrogen oxides in the global upper troposphere: interpreting cloud-sliced NO<sub>2</sub> observations from the OMI satellite instrument, *Atmospheric Chem. Phys.*, 18, 17017–17027, <https://doi.org/10.5194/acp-18-17017-2018>, 2018.



- 655 Marais, E. A., Roberts, J. F., Ryan, R. G., Eskes, H., Boersma, K. F., Choi, S., Joiner, J., Abuhassan, N., Redondas, A., Grutter, M., Cede, A., Gomez, L., and Navarro-Comas, M.: New observations of NO<sub>2</sub> in the upper troposphere from TROPOMI, *Atmospheric Meas. Tech.*, 14, 2389–2408, <https://doi.org/10.5194/amt-14-2389-2021>, 2021.
- McDuffie, E. E., Smith, S. J., O'Rourke, P., Tibrewal, K., Venkataraman, C., Marais, E. A., Zheng, B., Crippa, M., Brauer, M., and Martin, R. V.: A global anthropogenic emission inventory of atmospheric pollutants from sector- and fuel-specific sources (1970–2017): an application of the Community Emissions Data System (CEDS), *Earth Syst. Sci. Data*, 12, 3413–3442, <https://doi.org/10.5194/essd-12-3413-2020>, 2020.
- 660 Meng, J., Martin, R. V., Ginoux, P., Hammer, M., Sulprizio, M. P., Ridley, D. A., and Van Donkelaar, A.: Grid-independent high-resolution dust emissions (v1.0) for chemical transport models: application to GEOS-Chem (12.5.0), *Geosci. Model Dev.*, 14, 4249–4260, <https://doi.org/10.5194/gmd-14-4249-2021>, 2021.
- 665 Moxim, W. J., Levy, H., and Kasibhatla, P. S.: Simulated global tropospheric PAN: Its transport and impact on NO<sub>x</sub>, *J. Geophys. Res. Atmospheres*, 101, 12621–12638, <https://doi.org/10.1029/96JD00338>, 1996.
- Murphy, J. G., Thornton, J. A., Wooldridge, P. J., Day, D. A., Rosen, R. S., Cantrell, C., Shetter, R. E., Lefer, B., and Cohen, R. C.: Measurements of the sum of HO<sub>2</sub>NO<sub>2</sub> and CH<sub>3</sub>O<sub>2</sub>NO<sub>2</sub> in the remote troposphere, *Atmospheric Chem. Phys.*, 4, 377–384, <https://doi.org/10.5194/acp-4-377-2004>, 2004.
- 670 Murray, L. T., Jacob, D. J., Logan, J. A., Hudman, R. C., and Koshak, W. J.: Optimized regional and interannual variability of lightning in a global chemical transport model constrained by LIS/OTD satellite data, *J. Geophys. Res. Atmospheres*, 117, <https://doi.org/10.1029/2012JD017934>, 2012.
- Nault, B. A., Garland, C., Pusede, S. E., Wooldridge, P. J., Ullmann, K., Hall, S. R., and Cohen, R. C.: Measurements of CH<sub>3</sub>O<sub>2</sub>NO<sub>2</sub> in the upper troposphere, *Atmospheric Meas. Tech.*, 8, 987–997, <https://doi.org/10.5194/amt-8-987-2015>, 2015.
- 675 Nault, Benjamin. A., Garland, C., Wooldridge, P. J., Brune, W. H., Campuzano-Jost, P., Crouse, J. D., Day, D. A., Dibb, J., Hall, S. R., Huey, L. G., Jimenez, J. L., Liu, X., Mao, J., Mikoviny, T., Peischl, J., Pollack, I. B., Ren, X., Ryerson, T. B., Scheuer, E., Ullmann, K., Wennberg, P. O., Wisthaler, A., Zhang, L., and Cohen, R. C.: Observational Constraints on the Oxidation of NO<sub>x</sub> in the Upper Troposphere, *J. Phys. Chem. A*, 120, 1468–1478, <https://doi.org/10.1021/acs.jpca.5b07824>, 2016.
- 680 Ossohou, M., Galy-Lacaux, C., Yoboué, V., Hickman, J. E., Gardrat, E., Adon, M., Darras, S., Laouali, D., Akpo, A., Ouafu, M., Diop, B., and Opepa, C.: Trends and seasonal variability of atmospheric NO<sub>2</sub> and HNO<sub>3</sub> concentrations across three major African biomes inferred from long-term series of ground-based and satellite measurements, *Atmos. Environ.*, 207, 148–166, <https://doi.org/10.1016/j.atmosenv.2019.03.027>, 2019.
- Petzold, A., Thouret, V., Gerbig, C., Zahn, A., Brenninkmeijer, C. A. M., Gallagher, M., Hermann, M., Pontaud, M., Ziereis, H., Boulanger, D., Marshall, J., Nédélec, P., Smit, H. G. J., Friess, U., Flaud, J.-M., Wahner, A., Cammas, J.-P., Volz-Thomas, A., and Team, I.: Global-scale atmosphere monitoring by in-service aircraft – current achievements and future prospects of the European Research Infrastructure IAGOS, *Tellus B Chem. Phys. Meteorol.*, 67, 28452, <https://doi.org/10.3402/tellusb.v67.28452>, 2015.
- 685 Pickering, K. E., Wang, Y., Tao, W.-K., Price, C., and Müller, J.-F.: Vertical distributions of lightning NO<sub>x</sub> for use in regional and global chemical transport models, *J. Geophys. Res. Atmospheres*, 103, 31203–31216, <https://doi.org/10.1029/98JD02651>, 1998.
- Pinardi, G., Van Roozendaal, M., Hendrick, F., Theys, N., Abuhassan, N., Bais, A., Boersma, F., Cede, A., Chong, J., Donner, S., Drosoglou, T., Dzhola, A., Eskes, H., Frieß, U., Granville, J., Herman, J. R., Holla, R., Hovila, J., Irie, H., Kanaya, Y.,





- 695 Karagkiozidis, D., Kouremeti, N., Lambert, J.-C., Ma, J., Peters, E., Pöters, A., Postylyakov, O., Richter, A., Remmers, J., Takashima, H., Tiefengraber, M., Valks, P., Vlemmix, T., Wagner, T., and Wittrock, F.: Validation of tropospheric NO<sub>2</sub> column measurements of GOME-2A and OMI using MAX-DOAS and direct sun network observations, *Atmospheric Meas. Tech.*, 13, 6141–6174, <https://doi.org/10.5194/amt-13-6141-2020>, 2020.
- Poulida, O., Dickerson, R. R., and Heymsfield, A.: Stratosphere-troposphere exchange in a midlatitude mesoscale convective complex: 1. Observations, *J. Geophys. Res. Atmospheres*, 101, 6823–6836, <https://doi.org/10.1029/95JD03523>, 1996.
- 700 Reed, C., Evans, M. J., Di Carlo, P., Lee, J. D., and Carpenter, L. J.: Interferences in photolytic NO<sub>2</sub> measurements: explanation for an apparent missing oxidant?, *Atmospheric Chem. Phys.*, 16, 4707–4724, <https://doi.org/10.5194/acp-16-4707-2016>, 2016.
- Romer, P. S., Wooldridge, P. J., Crounse, J. D., Kim, M. J., Wennberg, P. O., Dibb, J. E., Scheuer, E., Blake, D. R., Meinardi, S., Brosius, A. L., Thames, A. B., Miller, D. O., Brune, W. H., Hall, S. R., Ryerson, T. B., and Cohen, R. C.: Constraints on Aerosol Nitrate Photolysis as a Potential Source of HONO and NO<sub>x</sub>, *Environ. Sci. Technol.*, 52, 13738–13746, <https://doi.org/10.1021/acs.est.8b03861>, 2018.
- 705 Ryan, R. G., Marais, E. A., Gershenson-Smith, E., Ramsay, R., Müller, J.-P., Tirpitz, J.-L., and Frieß, U.: Measurement report: MAX-DOAS measurements characterise Central London ozone pollution episodes during 2022 heatwaves, *Atmospheric Chem. Phys.*, 23, 7121–7139, <https://doi.org/10.5194/acp-23-7121-2023>, 2023.
- Ryerson, T. B., Williams, E. J., and Fehsenfeld, F. C.: An efficient photolysis system for fast-response NO<sub>2</sub> measurements, *J. Geophys. Res. Atmospheres*, 105, 26447–26461, <https://doi.org/10.1029/2000JD900389>, 2000.
- Scharko, N. K., Berke, A. E., and Raff, J. D.: Release of Nitrous Acid and Nitrogen Dioxide from Nitrate Photolysis in Acidic Aqueous Solutions, *Environ. Sci. Technol.*, 48, 11991–12001, <https://doi.org/10.1021/es503088x>, 2014.
- Schreier, S. F., Peters, E., Richter, A., Lampel, J., Wittrock, F., and Burrows, J. P.: Ship-based MAX-DOAS measurements of tropospheric NO<sub>2</sub> and SO<sub>2</sub> in the South China and Sulu Sea, *Atmos. Environ.*, 102, 331–343, <https://doi.org/10.1016/j.atmosenv.2014.12.015>, 2015.
- 715 SEAC4RS Science Team: SEAC4RS Field Campaign Data, <https://doi.org/10.5067/AIRCRAFT/SEAC4RS/AEROSOL-TRACEGAS-CLOUD>, 2014.
- Sen, P. K.: Estimates of the Regression Coefficient Based on Kendall's Tau, *J. Am. Stat. Assoc.*, 63, 1379–1389, <https://doi.org/10.1080/01621459.1968.10480934>, 1968.
- 720 Shah, V., Jacob, D. J., Dang, R., Lamsal, L. N., Strode, S. A., Steenrod, S. D., Boersma, K. F., Eastham, S. D., Fritz, T. M., Thompson, C., Peischl, J., Bourgeois, I., Pollack, I. B., Nault, B. A., Cohen, R. C., Campuzano-Jost, P., Jimenez, J. L., Andersen, S. T., Carpenter, L. J., Sherwen, T., and Evans, M. J.: Nitrogen oxides in the free troposphere: implications for tropospheric oxidants and the interpretation of satellite NO<sub>2</sub> measurements, *Atmospheric Chem. Phys.*, 23, 1227–1257, <https://doi.org/10.5194/acp-23-1227-2023>, 2023.
- 725 Silvern, R. F., Jacob, D. J., Travis, K. R., Sherwen, T., Evans, M. J., Cohen, R. C., Laughner, J. L., Hall, S. R., Ullmann, K., Crounse, J. D., Wennberg, P. O., Peischl, J., and Pollack, I. B.: Observed NO/NO<sub>2</sub> Ratios in the Upper Troposphere Imply Errors in NO-NO<sub>2</sub>-O<sub>3</sub> Cycling Kinetics or an Unaccounted NO<sub>x</sub> Reservoir, *Geophys. Res. Lett.*, 45, 4466–4474, <https://doi.org/10.1029/2018GL077728>, 2018.
- 730 Singh, H. B., Thompson, A. M., and Schlager, H.: SONEX airborne mission and coordinated POLINAT-2 activity: Overview and accomplishments, *Geophys. Res. Lett.*, 26, 3053–3056, <https://doi.org/10.1029/1999GL900588>, 1999.





- Singh, H. B., Brune, W. H., Crawford, J. H., Jacob, D. J., and Russell, P. B.: Overview of the summer 2004 Intercontinental Chemical Transport Experiment–North America (INTEX-A), *J. Geophys. Res.*, 111, D24S01, <https://doi.org/10.1029/2006JD007905>, 2006.
- 735 Stettler, M. E. J., Eastham, S., and Barrett, S. R. H.: Air quality and public health impacts of UK airports. Part I: Emissions, *Atmos. Environ.*, 45, 5415–5424, <https://doi.org/10.1016/j.atmosenv.2011.07.012>, 2011.
- Stratmann, G., Ziereis, H., Stock, P., Brenninkmeijer, C. A. M., Zahn, A., Rauthe-Schöch, A., Velthoven, P. V., Schlager, H., and Volz-Thomas, A.: NO and NO<sub>y</sub> in the upper troposphere: Nine years of CARIBIC measurements onboard a passenger aircraft, *Atmos. Environ.*, 133, 93–111, <https://doi.org/10.1016/j.atmosenv.2016.02.035>, 2016.
- Theil, H.: A Rank-Invariant Method of Linear and Polynomial Regression Analysis, *Indag. Math.*, 12, 1950.
- 740 Thompson, C. R., Wofsy, S. C., Prather, M. J., Newman, P. A., Hanisco, T. F., Ryerson, T. B., Fahey, D. W., Apel, E. C., Brock, C. A., Brune, W. H., Froyd, K., Katich, J. M., Nicely, J. M., Peischl, J., Ray, E., Veres, P. R., Wang, S., Allen, H. M., Asher, E., Bian, H., Blake, D., Bourgeois, I., Budney, J., Bui, T. P., Butler, A., Campuzano-Jost, P., Chang, C., Chin, M., Commane, R., Correa, G., Crouse, J. D., Daube, B., Dibb, J. E., DiGangi, J. P., Diskin, G. S., Dollner, M., Elkins, J. W., Fiore, A. M., Flynn, C. M., Guo, H., Hall, S. R., Hannun, R. A., Hills, A., Hints, E. J., Hodzic, A., Hornbrook, R. S., Huey, L. G., Jimenez, J. L., Keeling, R. F., Kim, M. J., Kupc, A., Lacey, F., Lait, L. R., Lamarque, J.-F., Liu, J., McKain, K., Meinardi, S., Miller, D. O., Montzka, S. A., Moore, F. L., Morgan, E. J., Murphy, D. M., Murray, L. T., Nault, B. A., Neuman, J. A., Nguyen, L., Gonzalez, Y., Rollins, A., Rosenlof, K., Sargent, M., Schill, G., Schwarz, J. P., Clair, J. M. St., Steenrod, S. D., Stephens, B. B., Strahan, S. E., Strode, S. A., Sweeney, C., Thames, A. B., Ullmann, K., Wagner, N., Weber, R., Weinzierl, B., Wennberg, P. O., Williamson, C. J., Wolfe, G. M., and Zeng, L.: The NASA Atmospheric Tomography (ATom) Mission: Imaging the Chemistry of the Global Atmosphere, *Bull. Am. Meteorol. Soc.*, 103, E761–E790, <https://doi.org/10.1175/BAMS-D-20-0315.1>, 2022.
- 745
- Toon, O. B., Maring, H., Dibb, J., Ferrare, R., Jacob, D. J., Jensen, E. J., Luo, Z. J., Mace, G. G., Pan, L. L., Pfister, L., Rosenlof, K. H., Redemann, J., Reid, J. S., Singh, H. B., Thompson, A. M., Yokelson, R., Minnis, P., Chen, G., Jucks, K. W., and Pszenny, A.: Planning, implementation, and scientific goals of the Studies of Emissions and Atmospheric Composition, Clouds and Climate Coupling by Regional Surveys (SEAC<sup>4</sup>RS) field mission, *J. Geophys. Res. Atmospheres*, 121, 4967–5009, <https://doi.org/10.1002/2015JD024297>, 2016.
- 755
- Torres, O., Bhartia, P. K., Jethva, H., and Ahn, C.: Impact of the ozone monitoring instrument row anomaly on the long-term record of aerosol products, *Atmospheric Meas. Tech.*, 11, 2701–2715, <https://doi.org/10.5194/amt-11-2701-2018>, 2018.
- Travis, K. R., Jacob, D. J., Fisher, J. A., Kim, P. S., Marais, E. A., Zhu, L., Yu, K., Miller, C. C., Yantosca, R. M., Sulprizio, M. P., Thompson, A. M., Wennberg, P. O., Crouse, J. D., St. Clair, J. M., Cohen, R. C., Laughner, J. L., Dibb, J. E., Hall, S. R., Ullmann, K., Wolfe, G. M., Pollack, I. B., Peischl, J., Neuman, J. A., and Zhou, X.: Why do models overestimate surface ozone in the Southeast United States?, *Atmospheric Chem. Phys.*, 16, 13561–13577, <https://doi.org/10.5194/acp-16-13561-2016>, 2016.
- 760
- Travis, K. R., Heald, C. L., Allen, H. M., Apel, E. C., Arnold, S. R., Blake, D. R., Brune, W. H., Chen, X., Commane, R., Crouse, J. D., Daube, B. C., Diskin, G. S., Elkins, J. W., Evans, M. J., Hall, S. R., Hints, E. J., Hornbrook, R. S., Kasibhatla, P. S., Kim, M. J., Luo, G., McKain, K., Millet, D. B., Moore, F. L., Peischl, J., Ryerson, T. B., Sherwen, T., Thames, A. B., Ullmann, K., Wang, X., Wennberg, P. O., Wolfe, G. M., and Yu, F.: Constraining remote oxidation capacity with ATom observations, *Atmospheric Chem. Phys.*, 20, 7753–7781, <https://doi.org/10.5194/acp-20-7753-2020>, 2020.
- 765
- Van Der Velde, I. R., Van Der Werf, G. R., Houweling, S., Eskes, H. J., Veeffkind, J. P., Borsdorff, T., and Aben, I.: Biomass burning combustion efficiency observed from space using measurements of CO and NO<sub>2</sub> by the TROPOspheric Monitoring Instrument (TROPOMI), *Atmospheric Chem. Phys.*, 21, 597–616, <https://doi.org/10.5194/acp-21-597-2021>, 2021.
- 770



- Van Der Werf, G. R., Randerson, J. T., Giglio, L., Collatz, G. J., Kasibhatla, P. S., and Arellano, A. F.: Interannual variability in global biomass burning emissions from 1997 to 2004, *Atmospheric Chem. Phys.*, 6, 3423–3441, <https://doi.org/10.5194/acp-6-3423-2006>, 2006.
- 775 Van Geffen, J., Eskes, H., Compornolle, S., Pinardi, G., Verhoelst, T., Lambert, J.-C., Sneep, M., Ter Linden, M., Ludewig, A., Boersma, K. F., and Veeffkind, J. P.: Sentinel-5P TROPOMI NO<sub>2</sub> retrieval: impact of version v2.2 improvements and comparisons with OMI and ground-based data, *Atmospheric Meas. Tech.*, 15, 2037–2060, <https://doi.org/10.5194/amt-15-2037-2022>, 2022.
- 780 Verhoelst, T., Compornolle, S., Pinardi, G., Lambert, J.-C., Eskes, H. J., Eichmann, K.-U., Fjæraa, A. M., Granville, J., Niemeijer, S., Cede, A., Tiefengraber, M., Hendrick, F., Pazmiño, A., Bais, A., Bazureau, A., Boersma, K. F., Bogner, K., Dehn, A., Donner, S., Elokhov, A., Gebetsberger, M., Goutail, F., Grutter de la Mora, M., Gruzdev, A., Gratsea, M., Hansen, G. H., Irie, H., Jepsen, N., Kanaya, Y., Karagkiozidis, D., Kivi, R., Kreher, K., Levelt, P. F., Liu, C., Müller, M., Navarro Comas, M., PETERS, A. J. M., Pommereau, J.-P., Portafaix, T., Prados-Roman, C., Puentedura, O., Querel, R., Remmers, J., Richter, A., Rimmer, J., Rivera Cárdenas, C., Saavedra de Miguel, L., Sinyakov, V. P., Stremme, W., Strong, K., Van Roozendaal, M., Veeffkind, J. P., Wagner, T., Wittrock, F., Yela González, M., and Zehner, C.: Ground-based validation of the Copernicus Sentinel-5P TROPOMI NO<sub>2</sub> measurements with the NDACC ZSL-DOAS, MAX-DOAS and Pandonia global networks, *Atmospheric Meas. Tech.*, 14, 481–510, <https://doi.org/10.5194/amt-14-481-2021>, 2021.
- 785 Vinken, G. C. M., Boersma, K. F., van Donkelaar, A., and Zhang, L.: Constraints on ship NO<sub>x</sub> emissions in Europe using GEOS-Chem and OMI satellite NO<sub>2</sub> observations, *Atmospheric Chem. Phys.*, 14, 1353–1369, <https://doi.org/10.5194/acp-14-1353-2014>, 2014.
- 790 Vohra, K., Marais, E. A., Bloss, W. J., Schwartz, J., Mickley, L. J., Van Damme, M., Clarisse, L., and Coheur, P.-F.: Rapid rise in premature mortality due to anthropogenic air pollution in fast-growing tropical cities from 2005 to 2018, *Sci. Adv.*, 8, eabm4435, <https://doi.org/10.1126/sciadv.abm4435>, 2022.
- 795 Wang, P., Stammes, P., Van Der A, R., Pinardi, G., and Van Roozendaal, M.: FRESCO+: an improved O<sub>2</sub> A-band cloud retrieval algorithm for tropospheric trace gas retrievals, *Atmospheric Chem. Phys.*, 8, 6565–6576, <https://doi.org/10.5194/acp-8-6565-2008>, 2008.
- 800 Wang, P.-H., Minnis, P., McCormick, M. P., Kent, G. S., and Skeens, K. M.: A 6-year climatology of cloud occurrence frequency from Stratospheric Aerosol and Gas Experiment II observations (1985-1990), *J. Geophys. Res. Atmospheres*, 101, 29407–29429, <https://doi.org/10.1029/96JD01780>, 1996.
- 805 Wang, Y., Dörner, S., Donner, S., Böhne, S., De Smedt, I., Dickerson, R. R., Dong, Z., He, H., Li, Z., Li, Z., Li, D., Liu, D., Ren, X., Theys, N., Wang, Y., Wang, Y., Wang, Z., Xu, H., Xu, J., and Wagner, T.: Vertical profiles of NO<sub>2</sub>, SO<sub>2</sub>, HONO, HCHO, CHOCHO and aerosols derived from MAX-DOAS measurements at a rural site in the central western North China Plain and their relation to emission sources and effects of regional transport, *Atmospheric Chem. Phys.*, 19, 5417–5449, <https://doi.org/10.5194/acp-19-5417-2019>, 2019.
- 810 Weng, H., Lin, J., Martin, R., Millet, D. B., Jaeglé, L., Ridley, D., Keller, C., Li, C., Du, M., and Meng, J.: Global high-resolution emissions of soil NO<sub>x</sub>, sea salt aerosols, and biogenic volatile organic compounds, *Sci. Data*, 7, 148, <https://doi.org/10.1038/s41597-020-0488-5>, 2020.
- van der Werf, G. R., Randerson, J. T., Giglio, L., van Leeuwen, T. T., Chen, Y., Rogers, B. M., Mu, M., van Marle, M. J. E., Morton, D. C., Collatz, G. J., Yokelson, R. J., and Kasibhatla, P. S.: Global fire emissions estimates during 1997–2016, *Earth Syst. Sci. Data*, 9, 697–720, <https://doi.org/10.5194/essd-9-697-2017>, 2017.



- Wild, O., Prather, M. J., and Akimoto, H.: Indirect long-term global radiative cooling from NO<sub>x</sub> Emissions, *Geophys. Res. Lett.*, 28, 1719–1722, <https://doi.org/10.1029/2000GL012573>, 2001.
- 815 Yang, L. H., Jacob, D. J., Colombi, N. K., Zhai, S., Bates, K. H., Shah, V., Beaudry, E., Yantosca, R. M., Lin, H., Brewer, J. F., Chong, H., Travis, K. R., Crawford, J. H., Lamsal, L. N., Koo, J.-H., and Kim, J.: Tropospheric NO<sub>2</sub> vertical profiles over South Korea and their relation to oxidant chemistry: implications for geostationary satellite retrievals and the observation of NO<sub>2</sub> diurnal variation from space, *Atmospheric Chem. Phys.*, 23, 2465–2481, <https://doi.org/10.5194/acp-23-2465-2023>, 2023.
- Ye, C., Zhang, N., Gao, H., and Zhou, X.: Photolysis of Particulate Nitrate as a Source of HONO and NO<sub>x</sub>, *Environ. Sci. Technol.*, 51, 6849–6856, <https://doi.org/10.1021/acs.est.7b00387>, 2017.
- 820 Zhao, B., Wang, S. X., Liu, H., Xu, J. Y., Fu, K., Klimont, Z., Hao, J. M., He, K. B., Cofala, J., and Amann, M.: NO<sub>x</sub> emissions in China: historical trends and future perspectives, *Atmospheric Chem. Phys.*, 13, 9869–9897, <https://doi.org/10.5194/acp-13-9869-2013>, 2013.
- Ziemke, J. R., Chandra, S., and Bhartia, P. K.: “Cloud slicing”: A new technique to derive upper tropospheric ozone from satellite measurements, *J. Geophys. Res. Atmospheres*, 106, 9853–9867, <https://doi.org/10.1029/2000JD900768>, 2001.
- 825 Zien, A. W., Richter, A., Hilboll, A., Blechschmidt, A.-M., and Burrows, J. P.: Systematic analysis of tropospheric NO<sub>2</sub> long-range transport events detected in GOME-2 satellite data, *Atmospheric Chem. Phys.*, 14, 7367–7396, <https://doi.org/10.5194/acp-14-7367-2014>, 2014.